A novel seismic strengthening method of RC columns confined by direct fastening steel plates

Z.W. Shan[a], D.T.W. Looi[b], R.K.L. Su[a,*]

[a]*Department of Civil Engineering, The University of Hong Kong, Pokfulam Road, Hong Kong, China*

[b]*School of Engineering, Swinburne University of Technology, Sarawak Campus, Sarawak, Malaysia*

Abstract

Reinforced concrete (RC) columns designed in accordance with older design codes that do not incorporate seismic resistance are prone to brittle failure. These defective columns may lead to the development of a non-ductile column sway mechanism during a strong earthquake. This failure process can be however remedied by strengthening the defective columns. In this study, an innovative strengthening method that uses direct fastening of steel plates is proposed for the seismic strengthening of RC columns. This method allows quick and easy implementation in practice, compared to the use of conventional steel jacketing connected through welding or bolting. The steel plates in the steel encasement can directly increase the axial, flexural and shear strengths. Furthermore, the confinement generated from the steel encasement can enhance the strength and ductility of the concrete core. This paper describes an experimental investigation of strengthened columns under reversed cyclic lateral load together with a constant vertical load and develops a theoretical model to predict the lateral capacity, which provides the basis for conducting the assessment of the generalized force-deformation relation. The experimental results indicate that the new connection method is robust and the strength and deformation of the strengthened columns are significantly improved. Variables such as connection

spacing, number of nails, steel plate thickness and axial load ratio can affect the mechanical behavior of the strengthened columns.

Keywords: RC column; seismic strengthening; steel plate; direct fastening; cyclic load.

1. Introduction

Recent post-earthquake investigations have shown that most reinforced concrete (RC) columns that were designed and built in accordance with older specifications that do not incorporate seismic design provisions fail to resist earthquake forces and cannot meet displacement demand, which has resulted in their collapse [1-4]. The collapse of such columns has meant great financial loss and damage to infrastructures and properties and even caused casualties. Hence, engineers have the option of incorporating seismic strengthening techniques for RC columns rather than opting for demolition-and-rebuild schemes. It should be noted that seismic strengthening techniques can be used to retrofit RC columns before earthquakes to comply with current national earthquake standards or repair such columns that have been subjected to post-earthquake damage. In this paper, the focus is on the former, i.e., retrofitting RC columns before an earthquake, as many buildings have been designed and constructed in accordance with older specifications, or in many low-to-moderate seismic regions where structures have not been seismically designed but earthquake design codes are introduced for the first time.

Previous experiments [5, 6] conducted on columns without considering seismicity have concluded that their strength and ductility are limited in comparison to columns that follow current design specifications. Furthermore, the non-seismic designed

columns in these frame buildings have not considered strength hierarchy (i.e., they do not include a capacity design principle [7]) and therefore the result is often an undesirable failure process due to strong-beam weak-column structural arrangements. These challenges can be circumvented by meeting specific targeted retrofitting objectives, that is, focusing on the flexural, shear or axial strengths, deformability or a combination of strength and deformability by resisting earthquake forces and meeting displacement demands through seismic codes of practices. Ideally, the seismic retrofitting techniques for RC columns can meet retrofitting objectives and are also practical; i.e., involves quick installation, reasonable cost, and durability.

One of the commonly used strengthening strategies for RC columns is RC jacketing [8-10]. Thermou et al. [10] conducted an experiment study on RC jacketed columns and found that their ductility and strength are noticeably enhanced, which is further observed in the work of Deng and Zhang [8] and Chang et al. [9]. The enhancement is attributed to the enlargement of the column section and the newly placed RC jacket which can partially offset the external load and provide confinement to the inner concrete. Nevertheless, the interface slip between the old and new concrete reduces the composite action of the strengthened columns [11]. To overcome this issue, various construction treatments have been tested including the use of concrete and shotcrete jackets [12, 13]. Furthermore, the construction of RC jackets is time and labor costs. Finally, the available amount of interior space can be reduced, and therefore RC jacketing is not recommended for metropolises like Hong Kong.

To avoid the shortcomings of RC jacketing, reinforced polymer jacketing which uses carbon fiber reinforced polymer (CFRP), basalt fiber reinforced polymer (BFRP), glass fiber reinforced polymer (GFRP) or textile has been researched and tested. These fiber-reinforced polymers have high elastic strength, which provides more confinement to concrete [14-18]. Wang et al. [19] studied the performance of

rectangular columns strengthened by CFRP jacketing which were subjected to lateral load in different directions. Rajput et al. [20] recently carried out testing on corroded RC columns restored by GFRP jacketing. Ma and Li [21] investigated the effect of BFRP on retrofitting damaged RC columns. Yin et al. [22] used textiles to reinforce concrete columns. They found that reinforced polymer jacketing is effective for increasing the energy dissipation and deformation capacity of columns that have been strengthened with textile-reinforced concrete. However, one controversial area of this strengthening method is its lack of fire resistance, which has greatly inhibited its widespread use. Furthermore, when textile-reinforced concrete is applied to rectangular columns with sharp corners, the stress is concentrated at the sharp corners [23].

Apart from the above methods, high-performance fiber reinforced cementitious composites (HPFRCCs) has been studied for strengthening RC columns. Li et al. [24] conducted experiments on four columns to examine the effectiveness of HPFRCCs. The results demonstrated that the lateral capacity and ductility are marginally increased when compared to the unrepaired columns. Cho et al. [25] improved on this method by combining additional steel bars. Although the effectiveness is enhanced, the section is enlarged and much more work is required to treat the concrete surface.

It can be observed that many distinct types of steel jacketing methods to strengthen RC columns have been proposed to overcome the inability of polymer-reinforced RC columns to resist fires and the enlarged cross-section problem using HPFRCCs strengthening method. Steel encasement strengthening can be classified as: wet strengthening and dry strengthening according to the contact between concrete and steel encasement. Wet strengthening has been studied since 1990s. Priestley et al. [26] first proposed an elliptical steel jacket. The large gap between steel jackets and column is infilled with concrete. Subsequently, Ghobarah et

al. [27] used welded corrugated steel jackets to strengthen the lap splice region. The gap between steel jackets and column is infilled with grout. Although strength and ductility are both improved by wet strengthening, it is hard to implement and the enlarged cross-section problem is not entirely overcome. This method is suitable to strengthen the bridge piers but not building frame columns. Lately, Choi et al. [28] proposed a method that excludes grouting but applying external pressure and welding to connect the jackets. On the contrary, the dry strengthening is easier to construct and saves on occupied floor area, however the incompatible deformation affects the performance of the strengthened column. To overcome this, mechanical anchors are used to achieve composite action [29,30]. However, precise holes which need to be drilled on steel plate to place the anchors, could be challenging. Also, drilling holes on column may damage the column and thus impair the strength of the column. Xu et al. [31] proposed a welded steel jacket strengthening method, however on-site vertical welding of thin steel plates is a laborious task and challenging to implement as the undertaking often requires a skillful welder. Also, it should be noted that welding can cause warping of the steel section due to non-uniformity of the heat transfer to the metal body.

In light of the challenges found with current strengthening methods, an innovative steel encasement is developed in this study to address the issues. The proposed novel steel encasement possesses three advantages: (1) It is a dry strengthening method but composite action is ensured; (2) Direct fastening connection is used instead of welding or bolt connection; (3) Axial load capacity, shear strength and flexural strength can be enhanced. An experiment is carried out, under which 8 columns are subjected to cyclic lateral load and constant axial load to examine the effectiveness of the proposed strengthening method. To investigate the integrity of the connections under the effects of the axial load ratio (ALR) and nail number, two different ALRs

and two and four nails are used in the connections. The ALR is defined as ALR=$N_o/A_g f_c'$, where N_o is the existing axial load that is acting on the RC column, A_g is the cross-sectional area of the RC column and f_c' is the cylinder strength of the concrete. In addition, the steel plate thickness and connection spacing are also included to investigate the effect of different configurations of the steel encasement. The local and post local buckling of steel encasement were found greatly affecting the performance of column [32]. Based on the experimental results, the following factors are examined: failure mode, hysteretic curve, envelope curve, dissipation of energy, secant stiffness degradation, shear force in the steel plate, effective stiffness and generalized force-deformation relation. A theoretical model is then developed for the strengthening method to predict the lateral load capacity which is validated with the experimental results. The normalized axial-moment (N-M) is plotted and then approximated by using a bi-linear model.

2. Experimental program

In this section, the configurations of the 8 RC column specimens tested in the structural laboratory of The University of Hong Kong, are discussed. The material properties of the concrete, steel bar and steel plates are reported. The details of the setup, loading protocols and instrumentation are also presented.

2.1. Configuration of the specimens

An un-strengthened RC column is shown in Figure 1, which is a prototype based on old low-rise buildings that were designed in accordance with old specification [33]. The column is scaled down to approximately one-third of its original size to fit the testing frame. Hence, RC columns with dimensions of $640\ \text{mm} \times 150\ \text{mm} \times 150\ \text{mm}$ and a length/width ratio of 4.3 were designed for

testing. The stirrup ratio and longitudinal steel rebar ratio are 0.3% and 1.4%, respectively, to simulate inadequate reinforcement of the columns.

Figure 2(a) shows the RC column strengthened by using the proposed steel encasement, in which a unique connection method is used between the height of the columns to connect the steel plates onto each of the adjacent column faces. The proposed steel encasement comprises four steel plates for the four faces of the columns. The strengthening procedure is as follows: Step 1: prefabrication of the steel jackets by welding the end angle bracket (where the size of the end angle bracket is 100 mm × 100 mm × 10 mm and the length is 120 mm) to the end of the steel plates; Step 2: the four steel plates are fastened to the top RC block and RC base of the specimen using anchor bolts. It is worth to note that the stiff end angle brackets can be fastened onto the floor and the bottom of RC beam by post-installed anchor in practical engineering projects; Step 3: the steel plates are tightly clamped to eliminate any gaps between the steel plates and RC columns. Also, the steel angle brackets for direct-fastening are fixed into place by using G-clamps to temporarily connect the two adjacent steel plates; and Step 4: the two adjacent steel plates are joined by direct fastening steel angle brackets, in which the right angle steel brackets (where the sizes of the direct fastening steel angle bracket is 70 mm × 70 mm × 5 mm and the length is 60 mm) and the steel plates can be tightly and quickly joined with high strength nails by using a powder-actuated tool; see Figure 2(b). The high strength nail, X-U 16 (with tensile strength of 2000 MPa) should only penetrate approximately 2 mm of the concrete cover to avoid crushing of the concrete. The details of this nail and its reliability as an integral part of this connection method have been discussed and verified previously in Shan and Su [34]. The proposed steel encasement not only partly supports the axial load on the column, but also increases the flexural strength of the column and enhances the deformability of the reinforcement. Additionally, the

direct fastening connections of the steel encasement may behave like transverse reinforcements, which would enhance the shear capacity.

Four variables, i.e., connection spacing, number of nails, steel plate thickness and the ALR, are considered in this study and expected to influence the cyclic behavior of the columns. These four variables are incorporated as the configurations of the 8 specimens as shown in Table 1 and Figure 3. The specimens are labeled as "C/S-ALR-t_p-s_d-n_f" where C represents the control columns and S represents the strengthened columns followed by the ALR, then the thickness of the steel plate, spacing of the connections and finally, the number of nails. Considering the requirement of axial stress limit stipulated in seismic design codes, e.g. EN 1998-1:2004 [35] which recommended a normalized design axial load (v_d) is required to be less than 0.65, where $v_d = N_{Ed}/A_g f_{cd}$. Readers are reminded to note the subtle difference of these axial stress limits stipulated in codes, where N_{Ed} denotes ultimate axial load and f_{cd} denotes design cylinder strength (i.e. characteristic cylinder strength with material factor of safety). However, the definition of ALR in this paper is ALR = $N_o/A_g f_c'$, where the unfactored axial load and mean cylinder strength are used. Thus, the normalized design axial load limit, 0.65, in EN 1998-1:2004 [35] is equivalent to ALR of 0.3 defined in this paper. Thus, two sets of ALRs (0.16 and 0.3) are used in this paper to investigate its effect on seismic performance. The only difference between S-0.16-4-100-2 and S-0.16-4-100-4 is the number of nails (2 vs. 4). Therefore, the effect of the number of nails was observed in a comparison between these two specimens. Besides, S-0.16-4-60-4 and S-0.16-4-100-4 are compared to determine the effects of spacing. Likewise, S-0.16-4-100-2, S-0.16-3-100-2 and S-0.16-5-100-2 are compared to determine the role of the steel plate thickness.

2.2. Material properties

A mild steel plate, a mild steel angle bracket and steel rebars were used in the testing. Three coupons were cut from mild steel angle bracket and the steel plate for each thickness in accordance with EN ISO 6892-1 [36]. They were tested in an MTS tensile machine at a loading rate of 1 mm / min. Three rebar samples with a length of 500 mm were cut from stirrups (R6) and a longitudinal rebar (T10), respectively and tested on the same tensile machine at a loading rate of 1 mm/min. The average yield strength, ultimate strength and the Young's modulus of the steel plates and steel rebars were determined and listed in Table 2.

The concrete was cast by following the mix proportion listed in Table 3. Note that the 8 specimens were consecutively cast as the same steel mould was used each time. Along with each specimen, 4 cylinders ($150\ \text{mm} \times 300\ \text{mm}$) and 2 cubes ($150\ \text{mm} \times 150\ \text{mm}$) were cast. Half of these were tested after the standard 28 days and the rest were tested on the same day as the column testing. The average cylinder strength (f_c') and cube strength (f_{cu}) are shown in Table 4. The transformation criterion broadly follows $f_c' \approx 0.8\, f_{cu}$.

2.3. Test setup and loading protocols

The setup shown in Figure 4 is able to simultaneously impose horizontal and axial loads by using 2 servo-controlled hydraulic actuators. The capacity of the actuators is 500 kN, where the horizontal actuator has a higher stroke of ± 250 mm and vertical actuator has a stroke of ± 150 mm. A steel box is bolted to the column so that it is attached to both the horizontal and vertical actuators. To control possible out-of-plane deflections and ensure in-plane deformation, a special frame and bracket assembly was designed. Two steel shoulder beams were placed on each side of the column base to fix the column in place and tightly fastened onto a rigid platform with eight Grade 10.9 high strength bolts.

The specimens were then subjected to cyclic horizontal and constant axial loading. The constant load was determined with the ALR and the cylinder strength tested on the same day during the column testing. It was noted that the vertical actuator is hinged and hence fluctuation during axial loading was unavoidable when the column deviated from its neutral position. Therefore, a tolerance of the load of ± 20 kN was allowed in the cyclic loading process. The axial load was also adjusted if it exceeded the prescribed range. To fully determine the cyclic behavior of the column, around 8 drift ratios for each column were calculated and two cycles were repeated for each drift ratio; see Figure 5. The stop criterion was reached when the lateral load was reduced to over 80% of the peak load.

2.4. Instrumentation

The horizontal force and horizontal displacement play a key role in analyzing the stiffness degradation and energy dissipation in each cycle and the ductility of the column. The horizontal force was automatically recorded by the control system while the displacement was measured by using linear variable displacement transducers (LVDTs); see Figure 6(a). The LVDTs are labeled as L1 to L10. The reference LVDTs, L2 and L3, are placed at the top of the column connected to the beam, which can be used to measure the horizontal displacement of the column. L1, L2 and L3 are used to examine if there is relative slip between the steel box and column. The column was fixed in place with two steel beams at the shoulders, which were fastened onto a rigid platform with high strength bolts. Hence, the uplift and slip were measured by L6, L7 and L8. When the drift ratio increased to the extent of its post peak value, column failure might occur; hence the axial displacement of the column was measured by L4 and L5.

The stress distribution in the longitudinal rebar, stirrups and steel plates

contributed to the development of the theoretical model for predicting the maximum horizontal load. As such, strain gauges S1 to S10 in Figure 1, were pre-installed prior to the concrete casting to measure the stress in the longitudinal rebars and stirrups. S11 to S20 (see Figure 6(b)) were placed to record the tensile and compressive stresses in the steel plate. Besides, rosette strain gauges (S21 to S26) were also mounted onto the steel plates to determine their shear stress (Figure 6(b)).

3. Experimental results

3.1. Failure modes

All eight samples were found to experience flexural failure, as evidenced from the crack patterns at the base, without any obvious diagonal shear cracks (Figure 7). It is also theoretically supported by the failure mode criterion stipulated in ASCE 41-13. That is when the ratio of plastic shear demand over the shear strength is less than 0.6, the flexural failure mode is then expected. The specific ratios of plastic shear demand over the shear strength for the eight samples are listed in Table 5, all of which are less than 0.6. The detailed theoretical derivation on the ratio of plastic shear demand over the shear strength is described in Section 5 in this paper. In the control column, C-0.3, several flexural cracks were found to be uniformly distributed along the column height. The plastic hinge region was identified at a distance of around 120 mm from the column base, which is about 0.8 d_c of the column and comparable to a distance of 112 mm which was predicted based on $L_p = 0.08L + 6\phi_l$, where L_p is the depth of the plastic hinge; L is the height of column; and ϕ_l denotes the diameter of the longitudinal rebar, as proposed in Priestley and Park [37].

Neither serious concrete spalling nor concrete crushing was observed in the

control columns; nevertheless, the columns could only undergo small drifting after reaching the peak lateral load prior to failure. On the contrary, critical flexural cracks were found in and around the plastic hinge region which was shifted upward in the strengthened columns, primarily due to the constraint of the end angle brackets. Concrete spalling and concrete crushing were also observed after the strengthened columns were tested under a large drift ratio. Bulging of the steel plates on the compressive side of the column was observed after reaching the peak lateral load. The connections play an important role in this strengthening method and were observed to be stable and robust during the entire loading process. It is worth noting that the steel plate detached from the RC column at the bottom of the tension fiber which was largely due to the effects of the stiff steel angle bracket placed at the bottom of the column which caused incompatibility of the steel jacket at the tension side during bending (see Figure 7). As a result, the assumption that the plane section would remain plane after deformation throughout the entire length of the column is inaccurate. Hence, a reduction factor was introduced for the tensile component of the steel plate when the lateral resistant capacity was estimated.

3.2. Hysteresis and envelope curves and deformability

The plotted hysteresis loops of the columns are shown in Figure 8, which includes the effect of the axial load. Minor fluctuations of the curves are due to the adjustment of the axial load. Prior reaching the peak lateral load, the two repeated hysteresis loops for each drift ratio almost overlap each other. After the peak lateral load is reached, the second hysteresis loop is different from the first hysteresis loop, where both the stiffness and the strength are reduced. However, after incorporating the proposed strengthening method, the strength and the deformability are both greatly increased. Besides, the pinching effect is reduced in the strengthened columns.

To better determine the effect of the variables (i.e., connection spacing, number of nails, steel plate thickness and ALR), the envelope curves of the first hysteresis loop for each drift ratio were extracted (see Figure 9) and the average maximum lateral load in the axial and lateral loading directions are listed in Table 5. The ultimate drift ratio when the lateral load is reduced to 80% of the maximum lateral load is also summarized in Table 5. For S-0.16-3-100-2, S-0.16-4-100-2, and S-0.16-5-100-2, the strength increases by 161%, 226%, and 268%, respectively and the ultimate drift ratio increases by 30%, 45%, and 80%, respectively when compared to the control column, C-0.16. This shows that the use of a thicker steel plate increases the strength and deformability of the strengthened columns. Besides, it can be observed that the effect of the number of nails is not significant, as even the minimum number of nails (2) can maintain the stability of the connections, and the observed failure is buckling at the steel plate and crushing of the concrete between the steel connections. Moreover, column failure is caused by the combined action of the lateral and axial loads. In this test, a larger ALR has an adverse effect on both the strength and deformability. With the application of the strengthening scheme, i.e. direct fastening steel plates, the ultimate drift ratio at an ALR of 0.3 (e.g. S-0.3-4-100-2) is comparable to that of the C-0.16 at an ALR of 0.16; see Figure 9(c). Furthermore, the strength of S-0.16-4-60-4 in increased more than that of S-0.16-4-100-4 and its ultimate drift ratio is also larger. The only difference between these two samples is the connection spacing. Less spacing can inhibit the buckling of the steel plate which contributes to the better performance of S-0.16-4-60-4.

3.3. Effective flexural stiffness and stiffness degradation

3.3.1. Effective flexural stiffness

Effective flexural stiffness is often considered in linear elastic structural analyses.

Therefore, the effective flexural stiffness of the strengthened RC columns is evaluated in this section. The effective flexural stiffness is determined by using [38,39]:

$$K_{ie} = \frac{0.2M_{\exp}}{\varphi_{0.2M\exp}} \tag{1}$$

where K_{ie} is the measured effective flexural stiffness; $M_{\exp}$ is the maximum bending moment which can be determined by the maximum lateral load times the force lever-arm; and $\varphi_{0.2M\exp}$ is the curvature of the column which is determined by the strain gauge that corresponds to a moment of $0.2M_{\exp}$.

In EN 1994-1-1:2004 [40] and AISC 360-16 [41], Equation (2a) is provided to examine the effective flexural stiffness of a composite column. The reduction factor is α_c, which is equal to a constant of 0.6 in EN 1994-1-1:2004 [40], and alternatively, obtained by using Equation (2b) in AISC 360-16 [41].

$$K_i = (EI)_s + \alpha_c (EI)_c \tag{2a}$$

$$\alpha_c = 0.45 + \frac{3A_{jacketing}}{A_c} \le 0.9 \tag{2b}$$

where $(EI)_s$ is the flexural stiffness provided by the steel jacketing; $(EI)_c$ is the flexural stiffness provided by the RC column; $A_{jacketing}$ is the cross-sectional area of the steel jacketing; A_c is the cross-sectional area of the RC column; and α_c is the reduction factor.

Comparisons of the predicted and measured effective flexural stiffnesses are listed in Table 6. The average ratio of the measured effective flexural stiffness over the effective flexural stiffness predicted based on EN 1994-1-1:2004 [40] is 0.93 and the coefficient of variation (COV) is 0.15. The measured effective flexural stiffness over the effective flexural stiffness predicted based on AISC 360-16 [41] is 0.88 and the

COV is 0.15. Therefore, the use of AISC 360-16 is not conservative enough, and EN 1994-1-1:2004 [40] is recommended in this study to predict the effective flexural stiffness of columns strengthened by direct-fastening steel plates.

3.3.2. Stiffness degradation

Figure 10 shows the reduction of the secant stiffness in the first cycle for each drift ratio. The secant stiffness for each drift ratio is normalized by the secant stiffness for the initial drift ratio. It can be seen that the residual secant stiffness is around 20% of the initial secant stiffness at the failure point. The use of the strengthening method can reduce the stiffness degradation. Therefore, the thickness of the steel plates has a negligible effect while the spacing of the connections has a more important role in governing the stiffness degradation. The secant stiffness of the strengthened columns with more closely spaced connections remains consistently higher for each drift ratio. In general, increasing the number of nails inhibits stiffness degradation while a larger ALR contributes to stiffness degradation.

3.4. Transverse shear force in steel plates

The shear strain and hence the shear force in the steel plates can be derived from the rosette strain gauge measurements. The transverse shear force in the steel plates was calculated at the maximum lateral load for all of the strengthened specimens and the results are shown in Figure 11. It can be seen that the transverse shear force in the steel plates can partly support more than 50% of the maximum lateral load. The steel plates on S-0.16-5-100-2 have the highest transverse shear force while those on S-0.16-3-100-2 have the lowest, which is because the steel jacket with a thickness of 5 mm can support a higher lateral load. The transverse shear force in the steel plates on S-0.16-4-60-4 is 28.2 kN which is slightly higher than the 25.1 kN of S-0.16-4-100-4,

which could be attributed to the different connection spacing. Steel jacketing with more closely spaced connections can support a higher lateral load. In this study, a larger ALR has an adverse effect on lateral resistance, which is why the transverse shear force in the steel plates on S-0.3-4-100-2 is lower than those on S-0.16-4-100-2.

3.5. Dissipated energy

The dissipated energy in the first cycle of loading of each specimen for each drift ratio is calculated and compared; see Figure 12. With a small drift ratio, there is minimal difference in the dissipated energy between the strengthened columns and non-strengthened columns. At this stage, the concrete significantly contributes to dissipating the energy while it is not seriously damaged. After the concrete is damaged from testing with a large drift ratio, the steel plate then plays the key role in dissipating energy with more obvious changes. That is, the difference in the amount of dissipated energy in the specimens that are fastened with steel plates of different thicknesses is negligible but those with a thicker steel jacket can support larger drifting before failure, which means that the steel jacket ensures that there is a sufficient capacity to dissipate energy. A slight difference between S-0.16-4-100-2 and S-0.16-4-100-4 can be observed in Figure 11(b). The difference between the two specimens is the number of nails in the connections, where there are 4 nails in the connections on S-0.16-4-100-4 which may produce a higher confinement effect to the concrete. The ability of S-0.16-4-60-4 which has a smaller connection spacing to dissipate energy excels that of S-0.16-4-100-4, as the buckling effect of the steel plate can be inhibited. More importantly, the ability to dissipate energy is preferred in strengthened specimens that are subjected to high axial loads at the same drift ratio. However, it is noted that this does not hold with a limited drift ratio; for example, the failure drift ratio of S-0.3-4-100-2 is approximately 2.0% while that of S-0.16-4-100-2

is about 3.5%.

3.6. Deformation behavior of steel plates

Given that the connections on the direct-fastening steel plates are rigid, the deformation of the steel plates thus governs the strengthening effect. The steel plate strains on both the tensile and compressive sides are summarized in Figure 13(a). Note that the end drift ratio on the tensile side corresponds to the stage of the maximum lateral load. It can be observed that almost all the cases reach the yield strain prior to the maximum lateral load except for S-0.3-4-100-2 with a larger ALR. On the compression side, it was found that steel plate buckling takes place before the maximum lateral load is reached and the buckling strain is very much affected by the slenderness ratio (λ_{sr}), which is defined as the connection spacing over the thickness of the steel plate and shown in Table 1. The buckling strain is reduced with a larger slenderness ratio; see Figure 13(a). For example, the buckling strain of S-0.16-4-60-4 with a slenderness ratio of 15 is -1300 microstrain (με) while that of S-0.16-3-100-2 with a slenderness ratio of 33.3 is -767 με. The buckling may be affected by initial imperfections, for example, there is initial bowing that resulted during the process of welding of the two end angle brackets onto each steel plate. To account for the issue, the Euler buckling theory was used and an imperfection factor was introduced by applying inverse calibration to the recorded buckling strain; see Figure 13(b). The buckling force in the steel plate is obtained by using:

$$P_{p,critical} = \frac{4\pi^2 D d_p}{s_d^2}(1-\alpha_i) \tag{3}$$

where α_i ($0 \le \alpha_i < 1$) is used to represent the initial imperfection factor. The equation $D = \frac{E_p t_p^3}{12(1-\mu_p^2)}$ is used to determine the bending stiffness of the steel plate

per unit width. E_p is the elastic modulus of the steel plate and μ_p is the Poisson's ratio of the steel plate. The thickness of the steel plate is t_p, while the depth of the steel plate is d_p.

The initial imperfection factor is given by:

$$\alpha_i = 1.06 - 0.009\lambda_{sr} \tag{4}$$

where λ_{sr} represents the slenderness ratio of the steel plate. Since the imperfection factor is calibrated with limited data and a slenderness ratio that ranges from 15 to 33.3, the proposed imperfection factor should be used within the tested slenderness ratios.

4. Theoretical development of flexural capacity of strengthened RC column

By the application of the plane section remaining plane, the strain profile of the strengthened RC column is illustrated in Figure 14. The stresses in the steel plate and longitudinal rebar can be determined by incorporating Hooke's law. However, the buckling of the steel plate under a compressive state is embedded. The tensile stress in the concrete is neglected and the rectangular stress block in the compression region is used. To accurately predict the stress in the two steel plates that are parallel to the loading direction, each is divided into *n* parts. The stresses in the steel plates and longitudinal rebar are determined with:

$$\varphi_c = \frac{\varepsilon_{cu}}{x_c} \tag{5a}$$

$$\sigma_{sc} = E_s(x_c - c - \frac{\phi_l}{2})\varphi_c; \sigma_{sc} \le f_{yl} \tag{5b}$$

$$\sigma_{pc1} = E_p(x_c + \frac{t_p}{2})\varphi_c; \sigma_{pc1} \le \min(f_{yp}, \frac{P_{p,critical}}{A_p}) \tag{5c}$$

$$\sigma_{st} = E_s(d_c - x_c - c - \frac{\phi_l}{2})\varphi_c; -f_{yl} \le \sigma_{st} \le f_{yl} \quad (5d)$$

$$\sigma_{pt1} = E_p(d_c - x_c + \frac{t_p}{2})\varphi_c; \max(-f_{yp}, -\frac{P_{p,critical}}{A_p}) \le \sigma_{pt1} \le f_{yp} \quad (5e)$$

$$\sigma_{pside\_i} = E_p(d_c - \frac{d_c - d_p}{2} - ((i-1)\frac{d_p}{n} + 2\frac{d_p}{n}) - x_c)\varphi_c; \max(-f_{yp}, -\frac{P_{p,critical}}{A_p}) \le \sigma_{pc2} \le f_{yp} \quad (5f)$$

where φ_c is the curvature of the column; x_c is the distance from the extreme compression fiber to the neutral axis of the RC column; ε_{cu} is the ultimate compressive strain of the concrete, which is equal to 0.003 based on ACI 318-14 [42]; σ_{sc} and σ_{st} are the compressive and tensile stresses in the longitudinal rebar; E_s represents the elastic modulus of the rebar; c is the concrete cover thickness; σ_{pc1} and σ_{pt1} are the stresses of the steel plates perpendicular to the lateral load; A_p is the cross-sectional area of the steel plates; f_{yp} is the yield stress of the steel plates; f_{yl} is the yield strength of the longitudinal rebar; and σ_{pside_i} is the stress of the i^{th} discrete element of the two steel plates parallel to the lateral load.

The two following expressions are derived based on the stress distribution profile shown in Figure 13 from the equilibrium of the axial load and taking moment of the extreme compressive fibers of the concrete:

$$N_0 + N_s + N_{p1} + 2N_{p2} - \alpha f_c' d_c \beta x_c = 0 \quad (6a)$$

$$N_0 \frac{d_c}{2} + M_s + M_{p1} + 2M_{p2} - \frac{1}{2}\alpha f_c' d_c (\beta x_c)^2 = V_{theo} l \quad (6b)$$

where

$N_s = 2\sigma_{st}A_l - 2\sigma_{sc}A_l$;

$N_{p1} = \eta_i \sigma_{pt1} A_p - \sigma_{pc1} A_p$;

$N_{p2} = \sum_{i=1}^{n} A_{pside\_i}\sigma_{pside\_i}$;

$$M_s = 2\sigma_{st}A_l(d_c - c - \frac{\phi_l}{2}) - 2\sigma_{sc}A_l(c + \frac{\phi_l}{2});$$

$$M_{p1} = \eta_i\sigma_{pt1}A_p(d_c + \frac{t_p}{2}) + \sigma_{pc1}A_p\frac{t_p}{2};$$

$$M_{p2} = \sum_{i=1}^{n} A_{pside\_i}\sigma_{pside\_i}(d_c - \frac{d_c - d_p}{2} - ((i-1)\frac{d_p}{n} + 2\frac{d_p}{n}));$$

where N_0 is the existing axial load that is acting on the RC column; N_s and M_s are the axial load and bending moment in the longitudinal rebar; N_{p1} and M_{p1} are the axial load and bending moment of the steel plates perpendicular to the lateral load; N_{p2} and M_{p2} are the axial load and bending moment of the steel plates parallel to the lateral load; a reduction factor of η_i=0.6 is introduced to compensate for the incompatibility of the deformation of the tensile steel plate perpendicular to the lateral load with the RC column, which is calibrated by ensuring the smallest relative error between the predicted peak lateral load and tested peak lateral load; A_{pside_i} is the discrete cross-sectional area of the steel plates parallel to the lateral load; A_l is the cross sectional area of the longitudinal rebar; l is the distance from the lateral load center to the base of the column for control columns or to the level of the cross section above the end angle bracket for strengthened columns; V_{theo} is the plastic shear capacity; and α and β are two factors used to describe the equivalent stress block of the concrete, which are equal to 0.85 in accordance with ACI 318-14 [42].

A comparison is made between the experimental and theoretical lateral loading capacity and the results are summarized in Table 6. Owing to the large lateral deformation at the peak lateral load, the second order effect cannot be neglected. The mean ratio of the theoretical lateral loading capacity over the experimental peak lateral load that considers the second order moment is 1.02 with a COV of 0.1.

The N-M interaction was then plotted based on the derived theoretical model. The

ordinate was normalized by using N_c ($N_c = (A_c - 4A_l) f_c^{'} + 4A_l f_{yl} + 4P_{p,critical}$) and the abscissa was normalized by using the moment capacity without the axial load M_0. The value of N_c can be supported with the data found in [43]. The average ratio of the predicted axial load capacity over that measured value is 0.93 with a COV of 0.02. An underestimation may be introduced by neglecting the confinement enhancement to the concrete by the steel encasement. The M_0 can be derived with Eq. (6) by neglecting the term of N_0 which is:

$$N_s + N_{p1} + 2N_{p2} - \alpha f_c' d_c \beta x_c = 0 \tag{7a}$$

$$M_s + M_{p1} + 2M_{p2} - \frac{1}{2}\alpha f_c' d_c (\beta x_c)^2 = M_0 \tag{7b}$$

The parameter values of S-0.16-4-60-4, S-0.16-3-100-2, S-0.16-4-100-2, and S-0.16-5-100-2 were then plotted to determine the effect of the slenderness ratio on the normalized N-M and the 6 experimental samples are superimposed in the same figure to further validate the model; see Figure 15. It can be observed in the figure that the effect of the slenderness ratio is negligible. Taking the point of the balanced failure O as the average of that of the four plotted curves, a simplified bi-linear model is proposed as follows to facilitate the application of the normalized N-M:

$$\frac{M}{M_0} - \frac{N}{2.4N_c} = 1; 0 \le \frac{N}{N_c} \le 0.12 \tag{8a}$$

$$\frac{0.84M}{M_0} + \frac{N}{N_c} = 1; 0.12 < \frac{N}{N_c} \le 1.0 \tag{8b}$$

where M and N are the moment and axial load that are acting on the columns.

5. Assessment of generalized force-deformation relation: ASCE 41-13

The effective flexural stiffness (as discussed earlier) is useful for linear elastic analyses; conversely, a generalized force-deformation relation; i.e., a backbone curve,

is often recommended for nonlinear analyses; see Figure 16. The generalized force-deformation relation has a linear deformation from Points A to B. From Points B to C, a linear relation with reduced stiffness is adopted and the reduced stiffness is equal to 0-10% of the initial stiffness. In this paper, the slope from Points B to C is equal to zero. Point C represents the maximum lateral load capacity. The DE Phase denotes the process from failure due to lateral load to axial failure and the residual strength is represented with *r*. After Point E, collapse takes place. The values of *a*, *b* and *r* are listed in Table 7, where they are influenced by the ALR, transverse reinforcement ratio and three conditions which are defined by the ratio of the plastic shear demand over the shear strength (V_{theo}/V_o). Condition (i) corresponds to $V_{theo}/V_o \leq 0.6$; Condition (ii) corresponds to $1.0 \geq V_{theo}/V_o \geq 0.6$; and Condition (iii) to $V_{theo}/V_o \geq 1.0$. The plastic shear capacity (V_{theo}) can be estimated based on the section with Equation 6(b) and the shear capacity (V_0) is determined in the following section.

5.1. Shear capacity of strengthened RC columns

According to the recommendations in ACI 318-14 [42], the shear capacity of the RC column is determined by using:

$$V_{rc} = V_c + V_s \tag{9}$$

where V_c is the shear capacity of the concrete and V_s is the shear capacity attributed to the stirrups. The two components can be derived by using:

$$V_c = 0.17\left(1 + \frac{N_0}{14A_c}\right)\lambda\sqrt{f_c'}\,d_c d_w \tag{10}$$

$$V_s = \frac{A_{st} f_{yst} d_w}{s_{st}} \tag{11}$$

where d_c signifies the width of the cross section; d_w denotes the depth of the cross section; A_{st} is the cross sectional area of the stirrups; f_{yst} is the yield strength of

the stirrups; and s_{st} denotes the spacing of the stirrups.

The function of the direct-fastening connections is analogous to that of the stirrups. For the RC column strengthened with the proposed method, the shear resistance produced from the connections should be included. To avoid overestimation of the shear resistance from the steel jacketing, a factor of 0.5 is introduced by following EN 1998-3:2005 [45]. This component of shear force at the connections is thus obtained by using:

$$V_d = 0.5 \frac{d_c}{s_d + d_d} 2F_d \tag{12}$$

where d_d is the length of the steel angle bracket, F_d represents the shear capacity of the connections and obtained by using [34]:

$$F_d = n_f \psi_{fp} \psi_{fk} \alpha_{br} d_n t_p f_{pu} \tag{13}$$

where α_{br} represents the bearing resistance factor, which is equal to 1.6 and ψ_{fp} denotes the factor for the protuberance effect. If there are pre-drilled holes on the connected steel plate, the bearing resistance factor is equal to 1.0; otherwise, 1.35. ψ_{fk} represents the effect of knurling and the value is equal to 1.17 for a knurled fastener; d_n is the diameter of the nail and f_{pu} represents the ultimate strength of the connected steel plate.

Combining the three shear strength components, the shear capacity of the strengthened RC column is determined by using:

$$V_0 = V_c + V_s + V_d \tag{14}$$

5.2. Evaluation of generalized force-deformation relation in ASCE 41-13

The ratios of the plastic shear demand over the shear strength conditions are summarized in Table 5, where all 8 columns are classified as Condition (i). It can be seen from Table 7 that the values of *a*, *b* and *r* are influenced by the transverse reinforcement ratio. In this strengthening scheme, there are two types of transverse

reinforcements (i.e., stirrups and connections). Therefore, two transverse reinforcement ratios (with and without the effect of the connections of the steel jacketing) were considered. The equivalent transverse reinforcement ratio that considers the effect of the connections is obtained with:

$$\rho_{veq} = \rho_v + \frac{F_d}{f_{yst} d_c (s_d + d_d)} \tag{15}$$

where ρ_v is the stirrup ratio.

In Figure 17, the generalized force-deformation relations are compared to the experimental results. A dashed line is drawn by neglecting the effect of the transverse confinement provided by the steel jacketing, but the effect is taken into consideration for the calculations shown by the solid red line. It can be seen that the former can appropriately address the overall behavior of RC columns S-0.16-4-100-4, S-0.16-4-100-2 and S-0.16-3-100-2; see Figures 17(b) to 17(d). The slenderness ratio of these samples is 25 and 33.3. However, the generalized force-deformation relation which neglects the effect of the transverse confinement provided by the steel jacket is conservative for S-0.16-4-60-4 (Figure 17(a)) and S-0.16-5-100-2 (Figure 17(e)), where the slenderness ratio is 15 and 20, respectively. Interestingly, the generalized force-deformation relation which considers the effect of the transverse confinement provided by the steel jacket matches well with the experiment results. It appears that the equivalent transverse reinforcement ratio is more suitable for representing the nonlinear behavior of the strengthened columns which have a small slenderness ratio of the steel jacket. In other words, a smaller slenderness ratio provides greater confinement effects.

In comparing the effects of the ALR for a similar configuration of retrofitted columns, i.e., S-0.16-4-100-2 (Figure 17(c)) and S-0.3-4-100-2 (Figure 17(f)), it was observed that the incorporation of the generalized force-deformation relations

recommended in ASCE41-13 [44] with the two components of the transverse reinforcements, that is, the stirrups and direct fastening connections, are not conservative enough for S-0.3-4-100-2 which has a larger ALR (Figure 17(f)). On the contrary, S-0.16-4-100-2 (Figure 17(c)) which has a smaller lower ALR, only the generalized force-deformation relations that take the stirrup ratio into consideration can appropriately envelope the force-deformation curves. Hence, it appears that the modelling parameters recommended in ASCE/SEI 41-13 [44] should be further tested under the influence of an ALR that is larger than 0.1 but smaller than 0.6 in Condition (i).

6. Conclusions

In this paper, a new strengthening method that uses direct-fastening steel plates is developed for RC columns. To evaluate the seismic performance of this proposed strengthening method, 8 specimens have been tested under cyclic lateral loads with a constant axial load. The main findings are summarized as follows:

(1) The lateral load capacity and ultimate drift ratio are significantly improved. For S-0.16-3-100-2, S-0.16-4-100-2, and S-0.16-5-100-2, the strength increased by 161%, 226%, and 268%, respectively and the ultimate drift ratio increased by 30%, 45%, and 80%, respectively when compared to the control column, C-0.16. For the two specimens subjected to an ALR of 0.3, the strength and the ultimate drift ratio of the strengthened specimen enhanced by 195% and 50% respectively, when compared with the unstrengthened column.

(2) A theoretical model has been developed for the strengthening method in this study and its effectiveness is validated with the experimental results. The normalized N-M is then plotted and approximated by using a bi-linear model.

(3) To facilitate a linear elastic analysis, the effective bending stiffness is examined and compared to the expressions in EN 1994-1-1:2004 [40] and AISC 360-16 [41], in which the former is recommended to predict the effective flexural stiffness of RC columns strengthened with direct fastening steel plates. On the contrary, to facilitate a nonlinear analysis, the RC columns are evaluated for a generalized force-deformation relation in accordance with ASCE/SEI 41-13 [44]. It appears that the use of an equivalent transverse reinforcement ratio is suitable for strengthening configurations with a small slenderness ratio and smaller ALR. However, the effect of a larger ALR (beyond 0.3) on the modelling parameters recommended in ASCE/SEI 41-13 [44] should be further investigated.

(4) The robustness of the connection construct with direct fastening to strengthen a column that is subjected to cyclic loads has been validated. The incompatibility of the deformation of the tensile steel plate perpendicular to the lateral load is examined and a reduction factor is used to quantify this effect. Buckling of the steel plates is observed and an imperfection factor is introduced to predict the buckling load.

References

[1] YY Wang. Lessons learned from the “5.12” Wenchuan Earthquake: evaluation of earthquake performance objectives and the importance of seismic conceptual design principles. Earthquake Engineering and Engineering Vibration 2008;7(3):255-262.

[2] H Sezen, AS Whittaker, KJ Elwood, KM Mosalam. Performance of reinforced concrete buildings during the August 17, 1999 Kocaeli, Turkey earthquake, and seismic design and construction practise in Turkey. Engineering Structures 2003:25(1):103-114.

[3] A Doğangün. Performance of reinforced concrete buildings during the May 1, 2003 Bingöl Earthquake in Turkey. Engineering Structures 2004; 26(6):841-856.

[4] D Mitchell, RH DeVall, M Saatcioglu, R Simpson, R Tinawi, R Tremblay. Damage to concrete structures due to the 1994 Northridge earthquake. Canadian Journal of Civil Engineering 1995; 22(2):361-377.

[5] SSE Lam, B Wu, YL Wong, ZY Wang, ZQ Liu, CS Li. Drift capacity of rectangular reinforced concrete columns with low lateral confinement and high-axial load. Journal of Structural Engineering 2003;129(6):733-742.

[6] K Skai, SA Sheikh. What Do We Know about Confinement in Reinforced Concrete Columns? (A Critical Review of Previous Work and Code Provisions). ACI Structural Journal 1989;86(2):192-207.

[7] MN Fardis. Capacity design: Early history. Earthquake Engineering and Structural Dynamics 2018;47(14):2887-2896.

[8] M Deng, Y Zhang. Cyclic loading tests of RC columns strengthened with high ductile fiber reinforced concrete jacket. Construction and Building Materials 2017;153:986-995.

[9] SY Chang, TW Chen, NC Tran, WI Liao. Seismic retrofitting of RC columns with RC jackets and wing walls with different structural details. Earthquake Engineering and Engineering Vibration 2014;13(2):279-292.

[10] GE Thermou, VK Papanikolaou, AJ Kappos. Flexural behaviour of reinforced concrete jacketed columns under reversed cyclic loading. Engineering Structures 2014;76:270-282.

[11] ENBS Júlio, FA Branco. Reinforced Concrete Jacketing--Interface Influence on Cyclic Loading Response. ACI Structural Journal 2008;105(4):471.

[12] KG Vandoros, SE Dritsos. Concrete jacket construction detail effectiveness when strengthening RC columns. Construction and Building Materials 2008;22(3):264-276.

[13] KG Vandoros, SE Dritsos. Interface treatment in shotcrete jacketing of reinforced concrete columns to improve seismic performance. Structural Engineering and

Mechanics 2006;23(1):43-61.

[14] QH Shen, JF Wang, JX Wang, ZD Ding. Axial compressive performance of circular CFST columns partially wrapped by carbon FRP. Journal of Constructional Steel Research 2019;155:90-106.

[15] QH Shen, JF Wang, QY Xu, YB Cui. Performance and design of partially CFRP-jacketed circular CFT column under eccentric compression. Journal of Constructional Steel Research 2020;166:105925.

[16] AW Al Zand, WHW Badaruzzaman, AA Mutalib, SJ Hilo. The enhanced performance of CFST beams using different strengthening schemes involving unidirectional CFRP sheets: An experimental study. Engineering Structures 2016;128:184-198.

[17] MI Alam, S Fawzia, XL Zhao, AM Remennikov, MR Bambach, M Elchalakani. Performance and dynamic behaviour of FRP strengthened CFST members subjected to lateral impact. Engineering Structures 2017;147:160-176.

[18] JF Wang, QH Shen, FQ Wang, W Wang. Experimental and analytical studies on CFRP strengthened circular thin-walled CFST stub columns under eccentric compression. Thin-Walled Structures 2018;127:102-119.

[19] D Wang, Z Wang, T Yu, H Li. Seismic performance of CFRP-retrofitted large-scale rectangular RC columns under lateral loading in different directions. Composite Structures 2018;192:475-488.

[20] AS Rajput, UK Sharma, K Engineer. Seismic retrofitting of corroded RC columns using advanced composite materials. Engineering Structures 2019;181:35-46.

[21] G Ma, H Li. Experimental study of the seismic behavior of predamaged reinforced-concrete columns retrofitted with basalt fiber–reinforced polymer. Journal of Composites for Construction 2015;19(6):04015016.

[22] S Yin, Y Yang, T Ye, Y Li. Experimental research on seismic behavior of reinforced concrete columns strengthened with TRC under corrosion environment. Journal of Structural Engineering 2016;143(5):04016231.

[23] YF Wu, T Liu, DJ Oehlers. Fundamental principles that govern retrofitting of reinforced concrete columns by steel and FRP jacketing. Advances in Structural Engineering 2006;9(4):507-33.

[24] X Li, J Wang, Y Bao, G Chen. Cyclic behavior of damaged reinforced concrete columns repaired with high-performance fiber-reinforced cementitious composite. Engineering Structures 2017;136:26-35.

[25] CG Cho, BC Han, SC Lim, N Morii, JW Kim. Strengthening of reinforced concrete columns by high-performance fiber-reinforced cementitious composite (hpfrc) sprayed mortar with strengthening bars. Composite Structures 2018;202: 1078-1086.

[26] MN Priestley, F Seible, Y Xiao. Steel jacket retrofitting of reinforced concrete bridge columns for enhanced shear strength--Part 2: Test results and comparison with theory. Structural Journal 1994;91(5):537-551.

[27] A Ghobarah, A Biddah, M Mahgoub. Rehabilitation of reinforced concrete columns using corrugated steel jacketing. Journal of Earthquake Engineering 1997;1(04):651-673.

[28] E Choi, YS Chung, K Park, JS Jeon. Effect of steel wrapping jackets on the bond strength of concrete and the lateral performance of circular RC columns. Engineering Structures 2013;48:43-54.

[29] CL Zhou, XW Li, DB Wang, SX Xia. Analysis of Bearing Capacity and Seismic Performance of Circular RC Columns Strengthened with Externally Wrapped Steel Plates. Advances in Civil Engineering 2019;2515091.

[30] RS Aboutaha, MD Engelhardt, JO Jirsa, ME Kreger. Retrofit of concrete columns

with inadequate lap splices by the use of rectangular steel jackets. Earthquake Spectra 1996;12(4):693-714.

[31] XC Xu, S Peng, J Deng, C Wan. Study on seismic behavior of encased steel jacket-strengthened earthquake-damaged composite steel-concrete columns. Journal of Building Engineering 2018;17:154-166.

[32] VI Patel, QQ Liang, MNS Hadi. Numerical analysis of high-strength concrete-filled steel tubular slender beam-columns under cyclic loading. Journal of Constructional Steel Research 2014;92:183-194.

[33] BSI, CP114. The structural use of reinforced concrete in Buildings. The Council for Codes of Practice, British Standards Institution, London; 1969.

[34] ZW Shan, RKL Su. Behavior of shear connectors joined by direct fastening. Engineering Structures 2019;196:109321.

[35] EN 1998-1:2004. Design of structures for earthquake resistance. Part 1: general rules, seismic actions and rules for buildings. CEN (European Committee for Standardization), 2004.

[36] EN ISO 6892-1: 2016. Metallic materials - Tensile testing. Part 1: Method of test at room temperature, CEN(European Committee for Standardization), 2016.

[37] MJN Priestley, R Park. Strength and ductility of concrete bridge columns under seismic loading. ACI Structural Journal 1987;84(1):61-76.

[38] AH Varma, JM Ricles, R Sause, LW Lu. Seismic behavior and modeling of high strength composite concrete-filled steel tube (CFT) beam–columns. Journal of Constructional Steel Research 2002;58(5):725–58.

[39] FY Liao, LH Han, Z Tao, KJ Rasmussen. Experimental behavior of concrete-filled stainless steel tubular columns under cyclic lateral loading. Journal of Structural Engineering ASCE 2016;143(4):04016219.

[40] European Committee for Standardization. EN 1994-1-1:2004. Design of

composite steel and concrete structures. Part 1–1: general rules and rules for buildings. CEN (European Committee for Standardization); 2004.

[41] American Institute of Steel Construction. ANSI/AISC 360-16. Specification for structural steel buildings. Chicago: American Institute of Steel Construction (AISC); 2016.

[42] ACI Committee 318. Building code requirements for structural concrete (ACI 318M-14) and commentary (ACI 318RM-14). Farmington Hills, MI: American Concrete Institute; 2015.

[43] RKL Su, ZW Shan. Axial strengthening of RC columns by steel encasement with direct fastening connections. IOP Conference Series: Materials Science and Engineering 2019;660(1):012055.

[44] American Society of Civil Engineers. ASCE/SEI 41-13. Seismic Evaluation and Retrofit of Existing Buildings. ASCE Standard. Reston, Virginia, US; 2014.

[45] European Committee for Standardization. EN 1998-3:2005. Design of structures for earthquake resistance – Part 3: assessment and retrofitting of buildings. European Committee for Standardization, CEN, Brussels, Belgium; 2005.

Symbols

n_{f}	number of nails in connection
s_{d}	connection spacing
d_d	the length of the connection angle
f_{c}'	cylinder strength
f_{cu}	cube strength
K_{ie}	measured effective flexural stiffness
$M_{\exp}$	maximum bending moment
$\varphi_{0.2M\exp}$	curvature of column that corresponds to moment of $0.2M_{\exp}$
$(EI)_s$	flexural stiffness provided by steel jacketing
$(EI)_c$	flexural stiffness provided by RC column
$A_{jacketing}$	cross-sectional area of steel jacketing
A_c	cross-sectional area of RC column
α_c	reduction factor in effective flexural stiffness
$P_{p,critical}$	buckling load in steel plate
α_i	initial imperfection factor
D	bending stiffness of steel plate per unit width
E_p	elastic modulus of steel plate
μ_p	Poisson's ratio of steel plate
t_p	thickness of steel plate
d_p	depth of steel plate
λ_{sr}	slenderness ratio of steel plate
φ_c	curvature of column
x_c	distance from extreme compression fiber to neutral axis of RC column
ε_{cu}	ultimate compressive strain of concrete
σ_{sc}	compressive stress of longitudinal rebar
σ_{st}	tensile stress of longitudinal rebar
E_s	elastic modulus of rebar
c	concrete cover thickness
ϕ_l	diameter of longitudinal rebar
σ_{pc1}, σ_{pt1}	stress of steel plates perpendicular to lateral load
A_p	cross-sectional area of steel plate
A_l	cross-sectional area of longitudinal rebar
f_{yp}	yield stress of steel plate
f_{yl}	yield stress of longitudinal rebar
σ_{pside_i}	stress of i^{th} discrete element of two steel plates parallel to lateral load
σ_{pside}	stress of two steel plates parallel to lateral load

N_0	existing axial load that is acting on RC column
N_s	axial load in longitudinal rebar
M_s	bending moment in longitudinal rebar
N_{p1}	axial load of steel plate perpendicular to lateral load
M_{p1}	bending moment of steel plate perpendicular to lateral load
N_{p2}	axial load of steel plate parallel to lateral load
M_{p2}	bending moment of steel plate parallel to lateral load
η_i	reduction factor to compensate for incompatibility of deformation of tensile steel plate with RC column
A_{pside_i}	discrete cross-sectional area of steel plate parallel to lateral load
l	distance from lateral load center to base of column
α , β	two factors to describe equivalent stress block of concrete
N_c	axial load capacity of column
M_0	moment capacity without axial load
M	moment on column
N	axial load on column
V_{theo}	lateral load capacity
V_o	shear capacity of column
V_{exp}'	experimental lateral load that considers second moment
V_{exp}	experimental maximum lateral load
K_{i_AISC}	effective flexural stiffness predicted in accordance with AISC 360-16
K_{i_EN}	effective flexural stiffness predicted in accordance with EN 1994-1-1:2004
L	height of column
L_p	depth of plastic hinge
d_c	width of column
V_c	shear capacity of concrete
V_s	shear capacity attributed to stirrups
d_w	depth of cross section
A_{st}	cross section area of stirrups
f_{yst}	yield strength of stirrups
s_{st}	spacing of stirrups
V_d	component of shear force at connections
F_d	shear capacity of connection
α_{br}	bearing resistance factor
ψ_{fp}	factor for protuberance effect
ψ_{fk}	effect of knurling
d_n	nail diameter

f_{pu}	ultimate strength of connected steel plate
V_{rc}	shear capacity of RC column
V_0	shear capacity of strengthened RC column
ρ_{veq}	equivalent transverse reinforcement ratio
ρ_v	stirrup ratio
l_d	limb length of steel angle bracket
ε_{pt1}, ε_{pc1}	strain of steel plate perpendicular to lateral load
ε_{sc}	compressive strain of longitudinal rebar
ε_{st}	tensile strain of longitudinal rebar
ε_{pside_i}	strain of i^{th} discrete element of two steel plates parallel to lateral load
a,b,g,r	parameter values on generalized force-deformation curve
v_d	normalised design axial load
N_{Ed}	ultimate axial load
f_{cd}	design cylinder strength

Table 1 Configuration of tested columns

Sample name	t_p (mm)	s_d (mm)	n_f	Nominal ALR	λ_{sr}	Remarks
C-0.16	-	-	-	0.16	-	Control for small ALR
S-0.16-3-100-2	3	100	2	0.16	33.3	Steel jacketing with thin steel plates
S-0.16-4-100-2	4	100	2	0.16	25	Connection with fewer nails
S-0.16-5-100-2	5	100	2	0.16	20	Steel jacketing with thick steel plates
S-0.16-4-60-4	4	60	4	0.16	15	Closer connection with more nails
S-0.16-4-100-4	4	100	4	0.16	25	Connection with more nails
C-0.3	-	-	-	0.3	-	Control for large ALR
S-0.3-4-100-2	4	100	2	0.3	25	Strengthened column with large ALR

Note: The steel plate thickness is t_p; s_d represents spacing between the adjacent connections; and n_f represents the number of fasteners in connection. L and d_c are the height and depth of the column, respectively. λ_{sr} is the slenderness ratio defined as the connection spacing over the thickness of the steel plate.

Table 2 Mechanical properties of rebars, steel plates and steel angle

Steel		Yield strength (MPa)	Ultimate strength (MPa)	Young's modulus (GPa)
Steel rebar	T10	586	671	187
	R6	394	514	206
Steel angle bracket	5 mm	305	420	205
Steel plate	3 mm	310	450	209
	4 mm	337	473	195
	5 mm	316	459	195

Table 3 Concrete mix proportion

Target cylinder strength (MPa)	Water/cement	Water (kg/m^3)	Cement (kg/m^3)	Sand (kg/m^3)	Aggregate (kg/m^3)	Superplasticizer (g/m^3)
20-30	0.7	249	356	1084.8	539.7	610

Table 4 Concrete strength

Sample	S1		S2		S3		S4		S5		S6		S7		S8	
No. of testing days	28	127	28	116	28	99	28	72	28	68	28	74	28	33	28	37
f_c' (MPa)	26	34.1	30.7	36	32.6	36.6	32.3	35.2	28.5	32.5	29.2	33.2	28.5	29.7	27.4	29.2
f_{cu} (MPa)	31.9	37.7	33.8	37.1	36.1	41	35.1	38.9	32.7	34.8	29.7	34.8	31.3	33.1	32.5	34.1

Note: concrete cylinder strength is denoted as f_c' and cube strength is denoted as f_{cu}.

Table 5 Shear capacity, ultimate drift ratio, axial load, experimental and theoretical lateral load

Specimen	Experimental lateral load (V_{exp})	Experimental lateral load that considers second moment (V_{exp}')	Axial load (kN)	Ultimate drift ratio	Shear capacity (V_o)	Theoretical lateral load (V_{theo})	V_{theo}/V_o	V_{theo}/V_{exp}'
C-0.16	13.0	14.7	155	2.0	47.5	15.9	0.28	1.08
S-0.16-3-100-2	33.9	37.6	177	2.6	89.1	35.7	0.37	0.95
S-0.16-4-100-2	42.4	47.9	207	2.8	105.5	45.1	0.41	0.94
S-0.16-5-100-2	47.9	55.3	227	3.6	119.4	53.2	0.42	0.96
S-0.16-4-60-4	44.0	49.2	277	3.2	234.4	48.9	0.2	0.99
S-0.16-4-100-4	41.3	46.2	215	3.0	161.2	45.6	0.27	0.99
C-0.3	11.2	12.6	267	1.2	51.7	14.7	0.28	1.17
S-0.3-4-100-2	31.8	37.2	375	1.8	97.2	40.0	0.36	1.08
Mean								1.02
COV								0.1

Note: V_{exp} is the experimental lateral load and V_{exp}' is the experimental lateral load that considers the second moment; V_o is the shear capacity; and V_{theo} is the theoretical lateral load.

Table 6 Effective bending stiffness

Specimen	K_{ie} (kN.m)	K_{i_AISC} (kN.m)	K_{i_EN} (kN.m)	K_{ie} / K_{i_AISC}	K_{ie} / K_{i_EN}
C-0.16	-	-	-		-
S-0.16-3-100-2	1926	1917	1840	1.0	1.05
S-0.16-4-100-2	1954	2416	2268	0.81	0.86
S-0.16-5-100-2	2184	2916	2696	0.75	0.81
S-0.16-4-60-4	1845	2416	2268	0.76	0.81
S-0.16-4-100-4	2074	2416	2268	0.86	0.91
C-0.3	-	-	-		-
S-0.3-4-100-2	2635	2416	2268	1.09	1.16
Mean				0.88	0.93
COV				0.15	0.15

Note: K_{ie} is the effective bending stiffness experimentally derived; K_{i_AISC} and K_{i_EN} are the effective bending stiffnesses predicted in accordance with AISC 360-16 [41] and EN 1994-1-1:2004 [40].

Table 7 Modeling parameters for nonlinear analysis based on ASCE 41-13 [44]

	ALR	ρ_v	Modeling parameter		
			a	*b*	*r*
Condition (i)	≤ 0.1	≥ 0.006	0.035	0.060	0.2
	≥ 0.6	≥ 0.006	0.010	0.010	0.0
	≤ 0.1	-0.002	0.027	0.034	0.2
	≥ 0.6	0.002	0.005	0.005	0.0

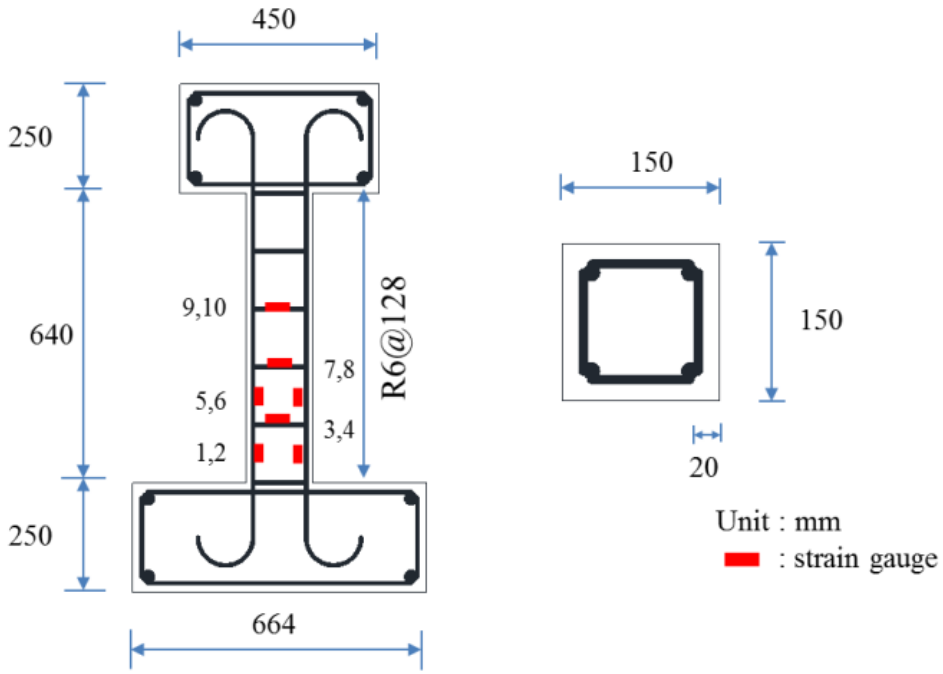

Fig. 1. Tested RC column

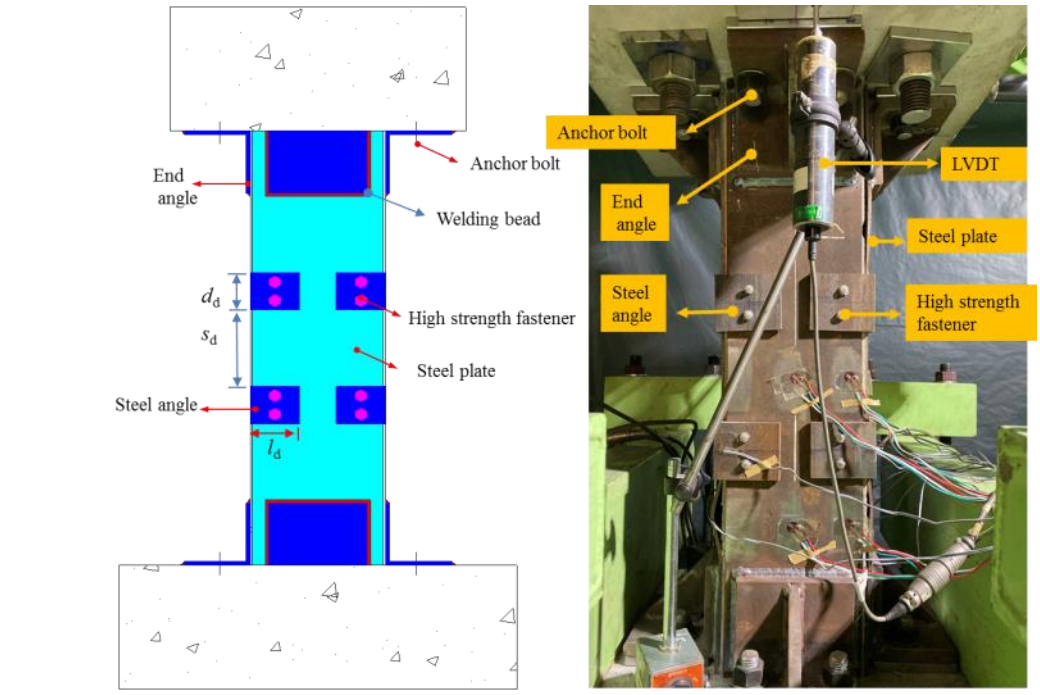

(a)

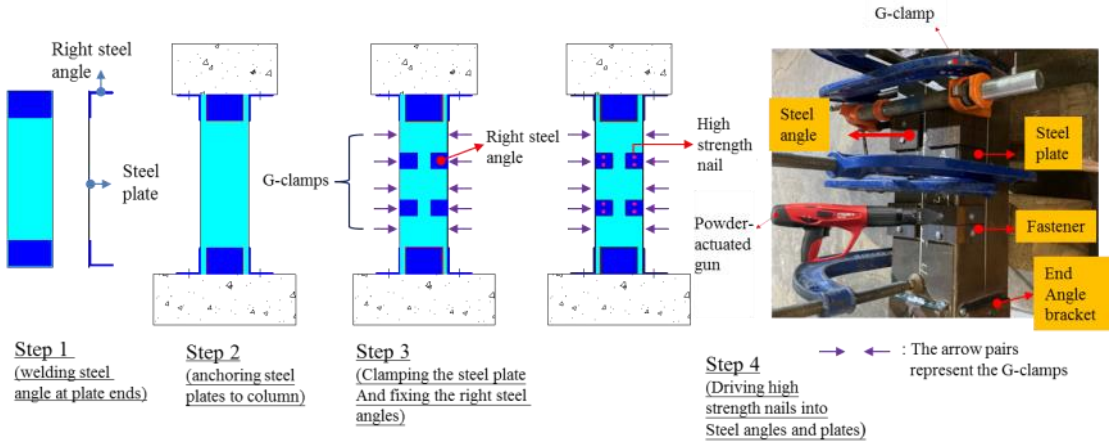

(b)

Fig. 2. Proposed strengthening method (a) strengthening schematic (b) strengthening procedure

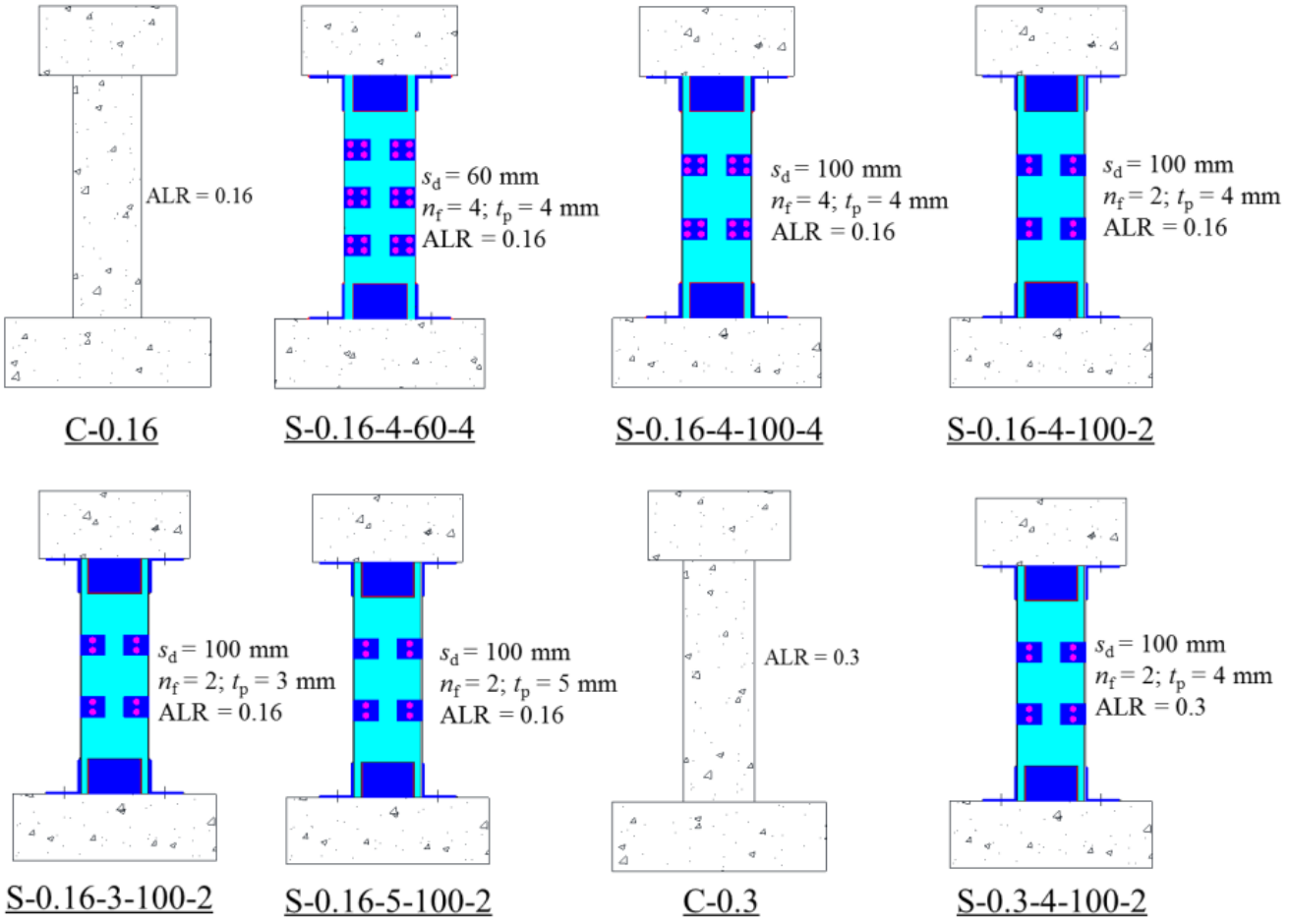

Fig. 3. Specimen configurations

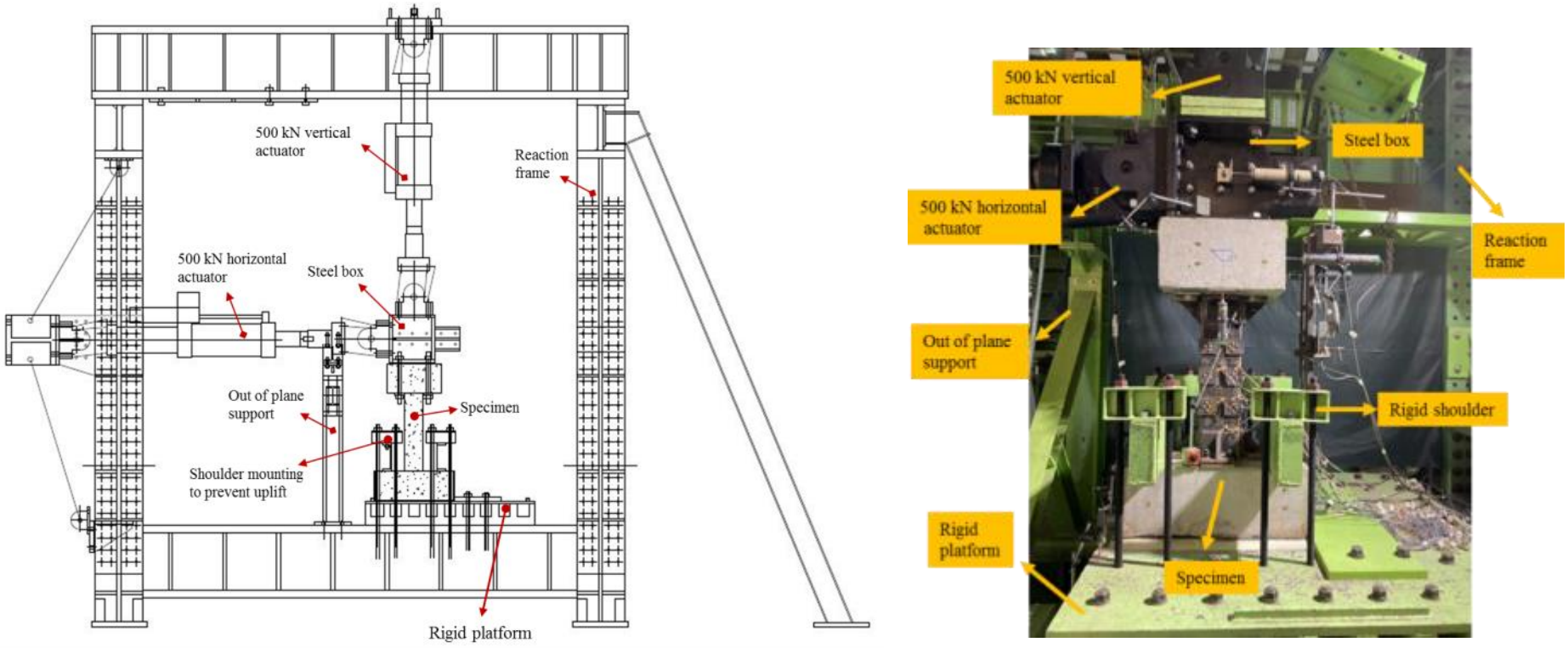

(a) (b)

Fig. 4. Test setup (a) front view and (b) specimen fitted onto test rig

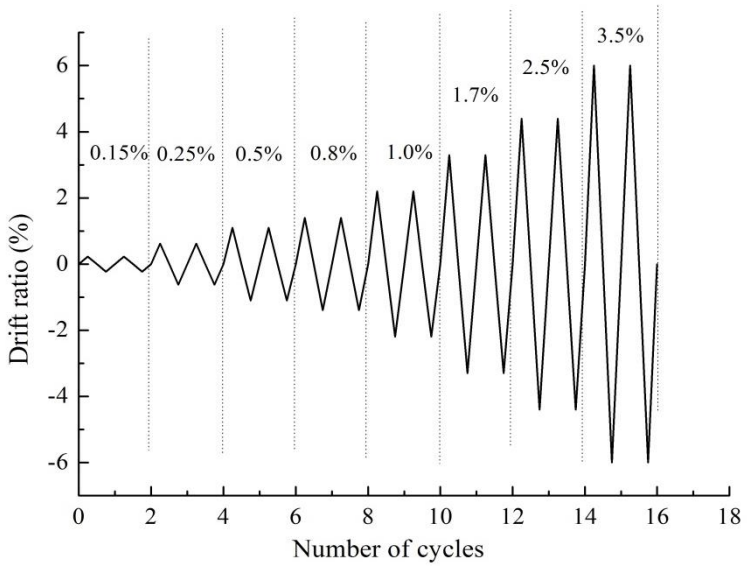

Fig. 5. Loading protocol

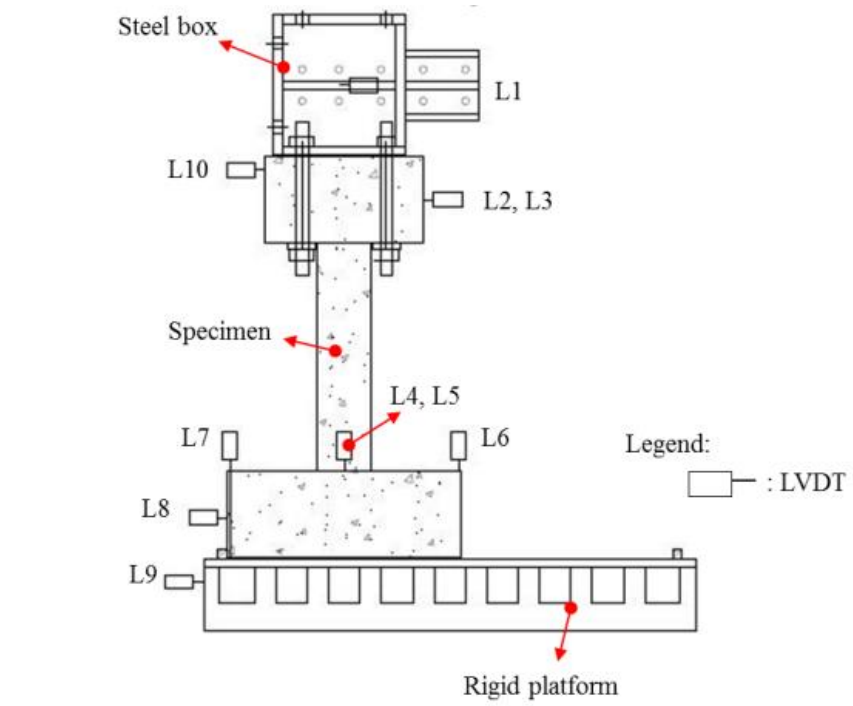

(a)

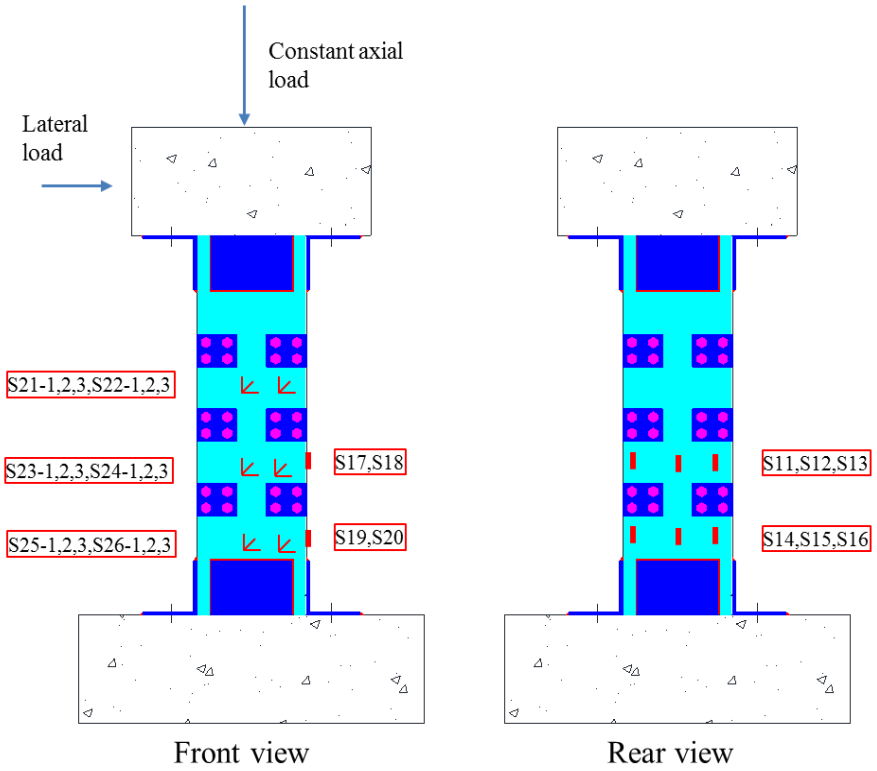

(b)

Fig. 6. (a) LVDTs arrangement and (b) strain gauge distribution

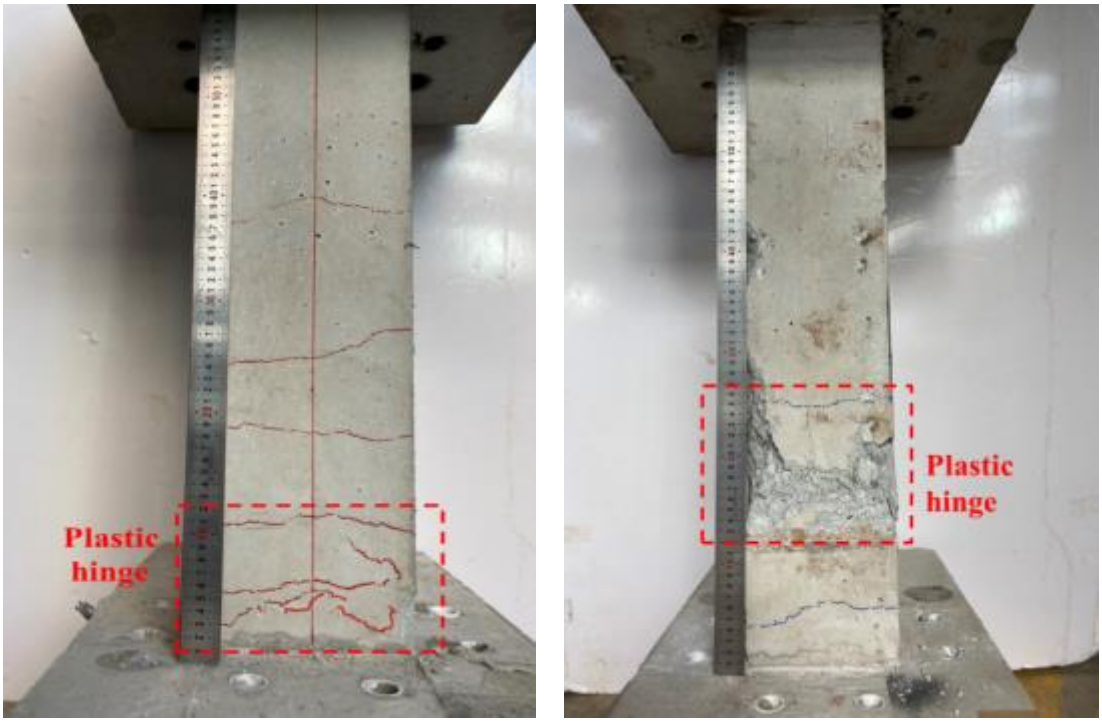

C-0.3 S-0.3-4-100-2

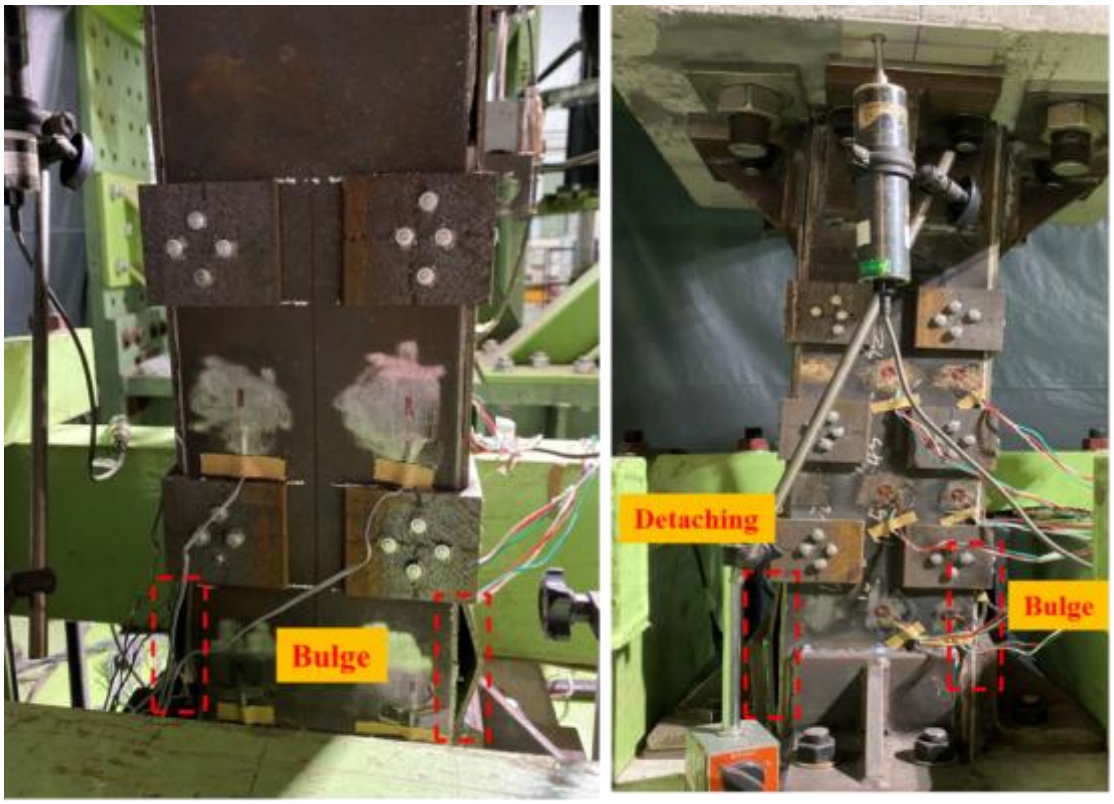

Side view Front view

Fig. 7. Failure modes of columns

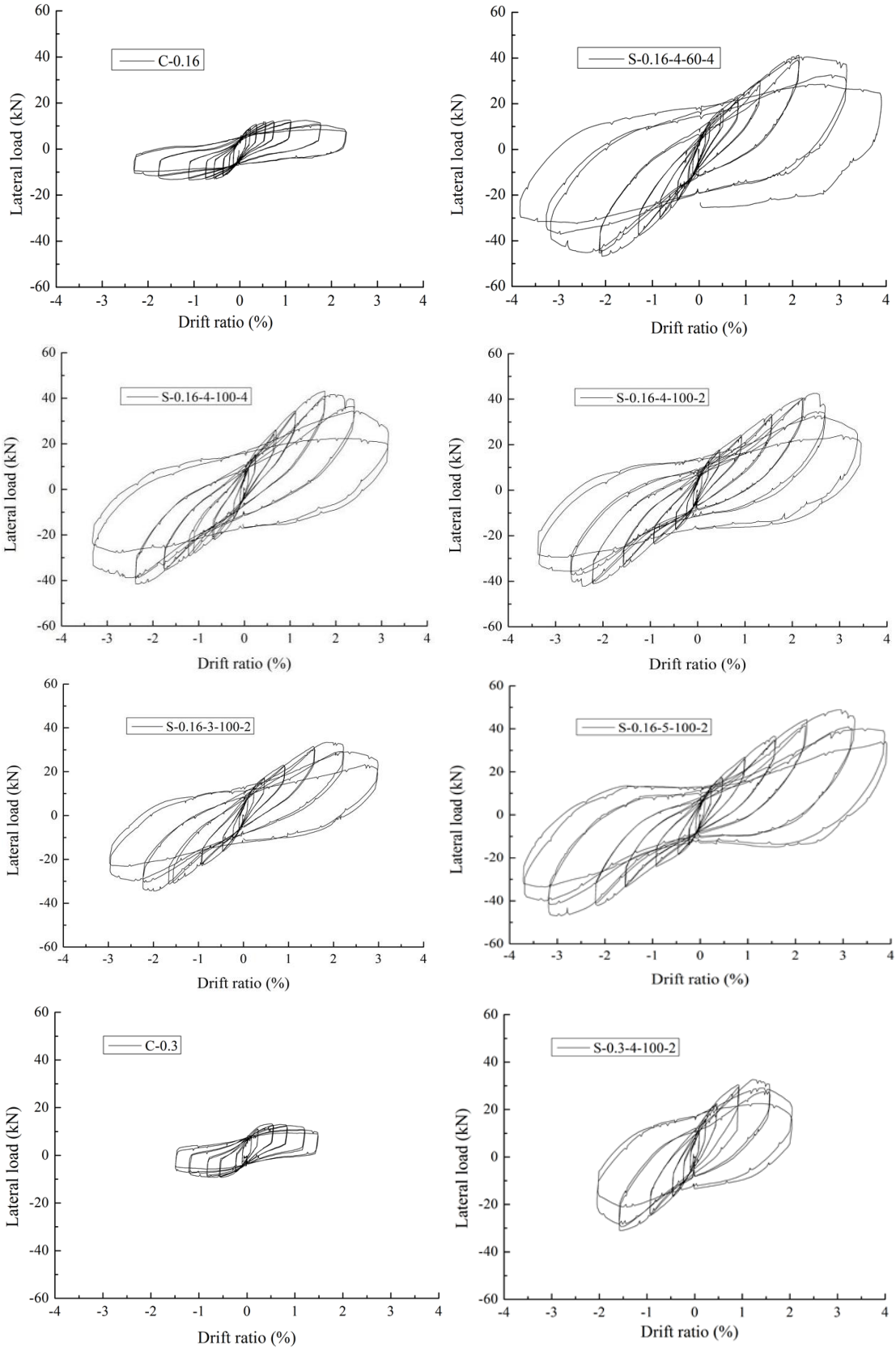

Fig. 8. Hysteretic curves

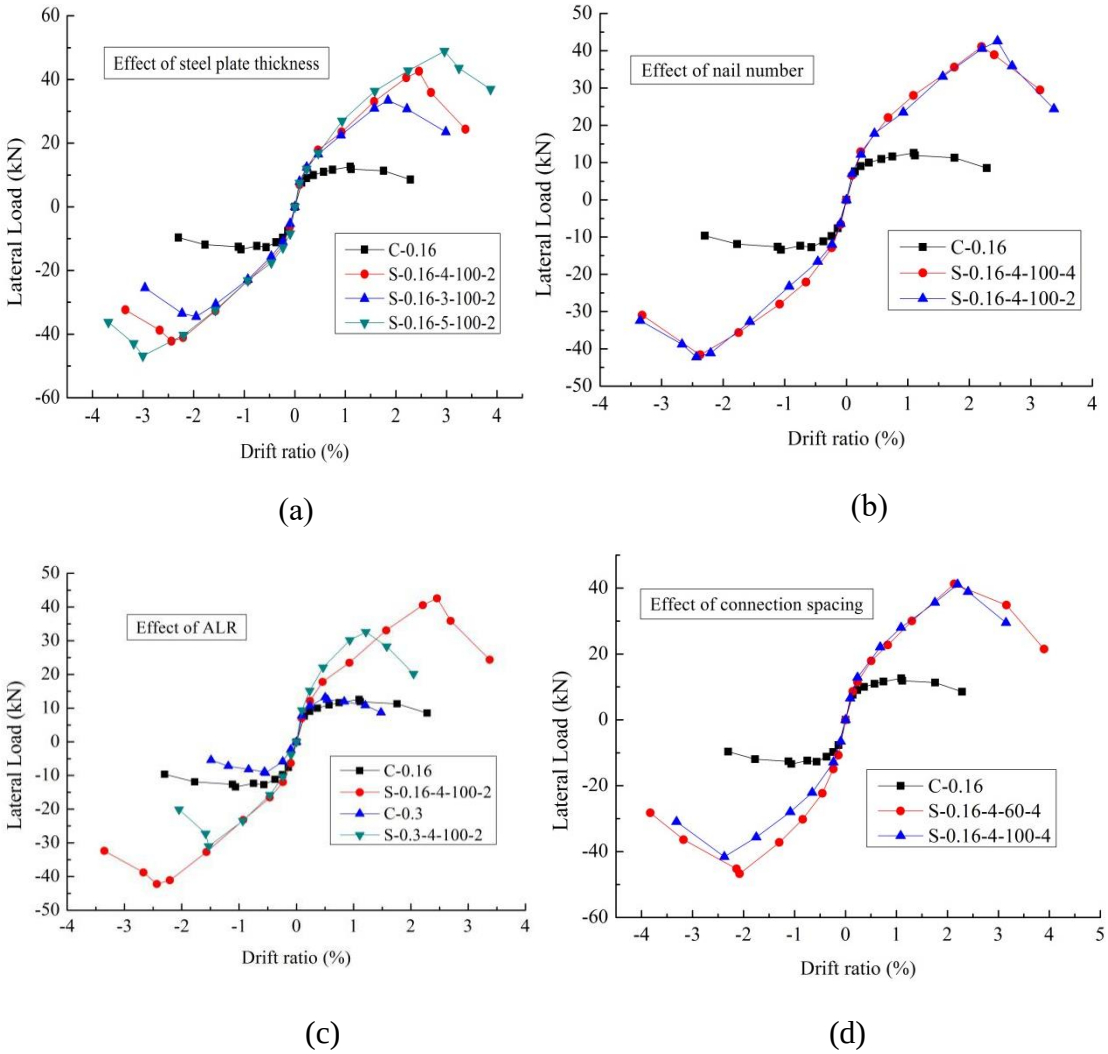

Fig. 9. Envelope curves: effect of (a) steel plate thickness, (b) number of nails, (c) ALR and (d) connection spacing

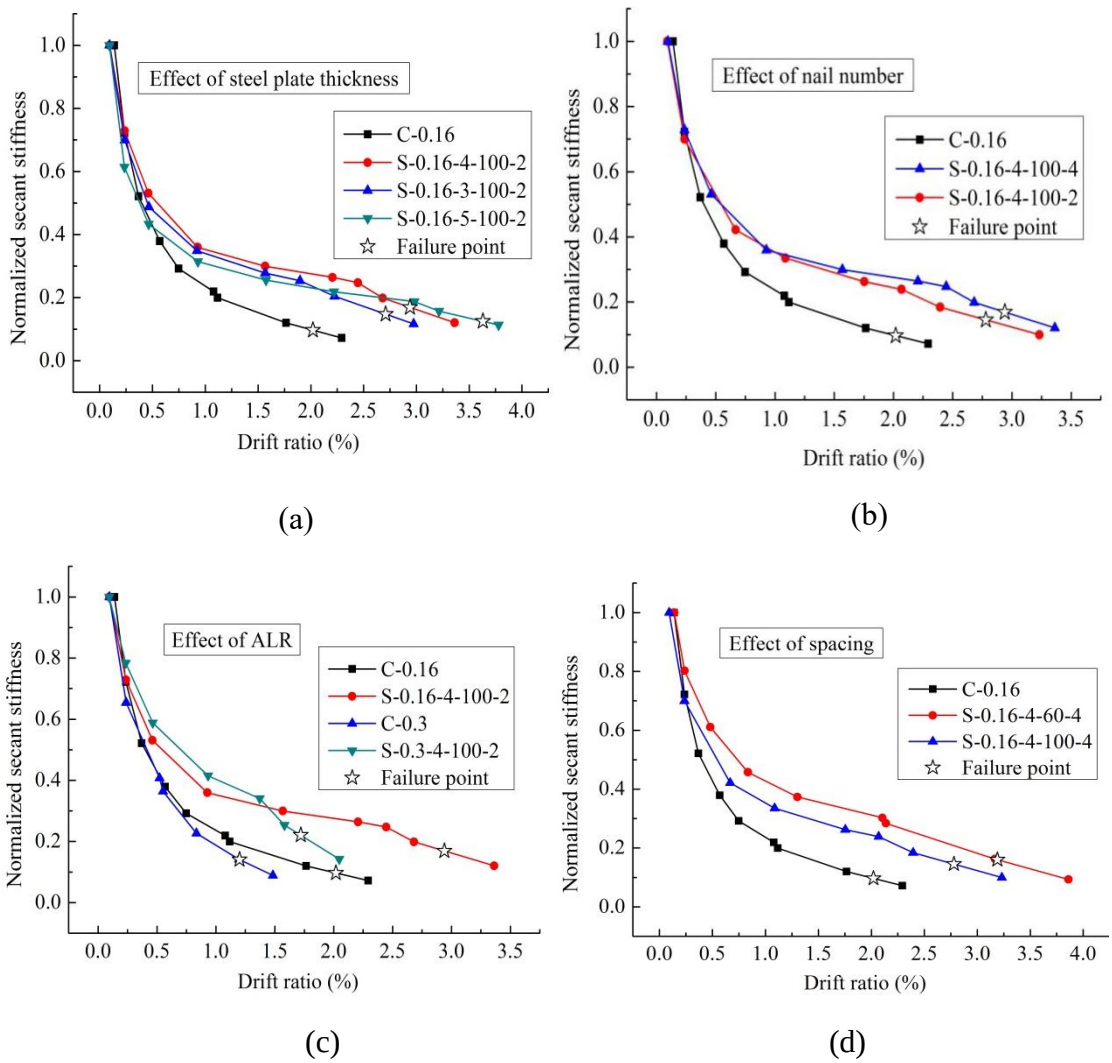

Fig. 10. Stiffness degradation: effect of (a) steel plate thickness, (b) number of nails, (c) ALR and (d) connection spacing

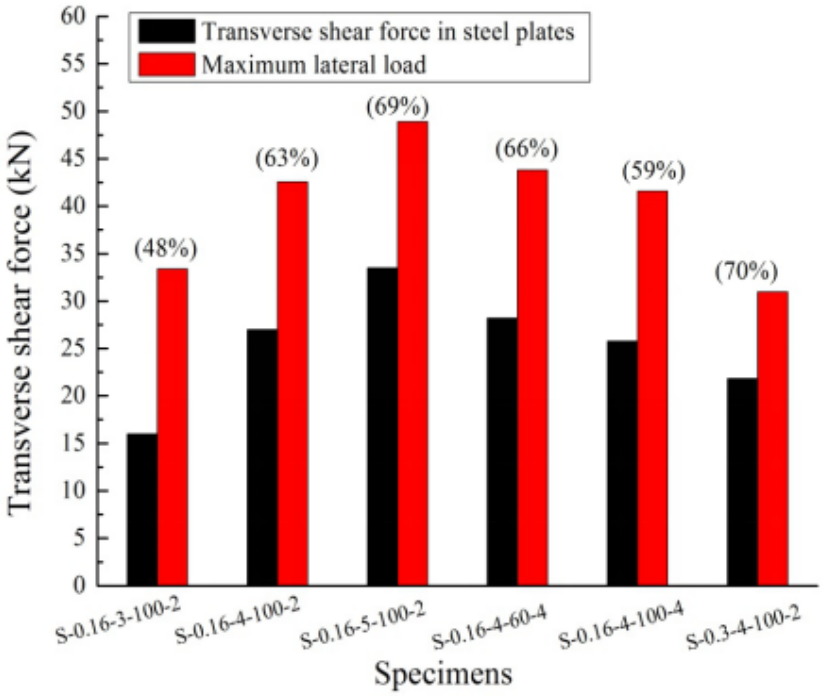

Fig. 11. Transverse shear force in steel plates

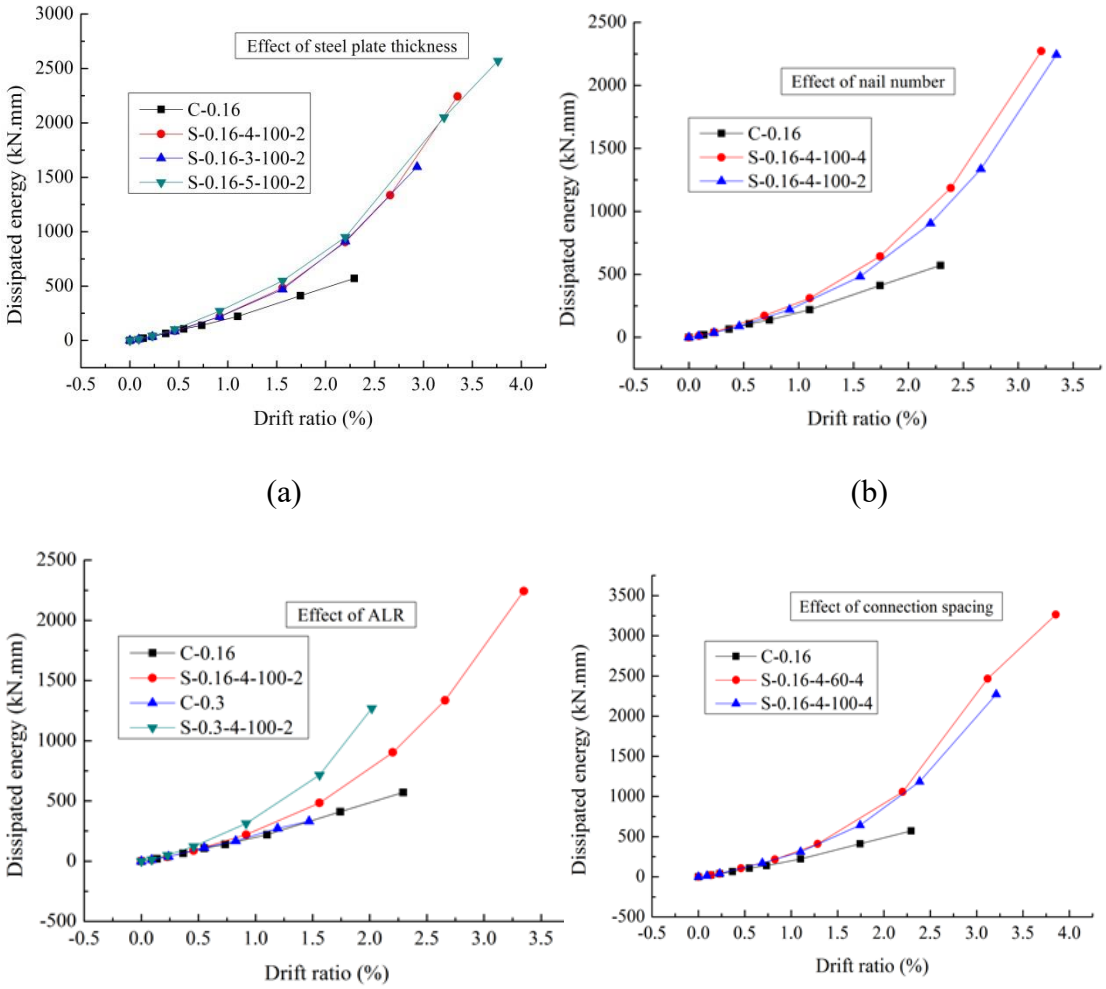

Fig. 12. Dissipated energy: effect of (a) steel plate thickness, (b) number of nails, (c) ALR and (d) connection spacing

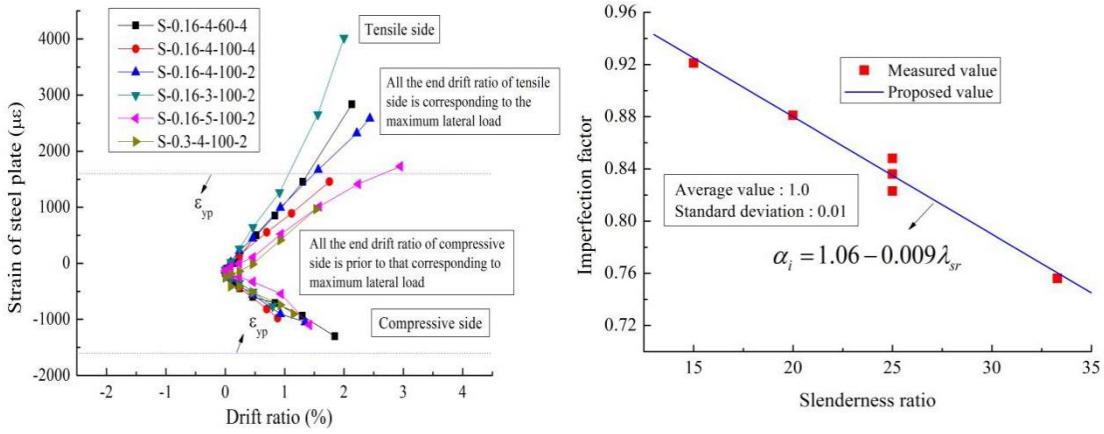

(a) (b)

Fig. 13. Behavior of steel plate (a) Longitudinal strain and (b) imperfection factor

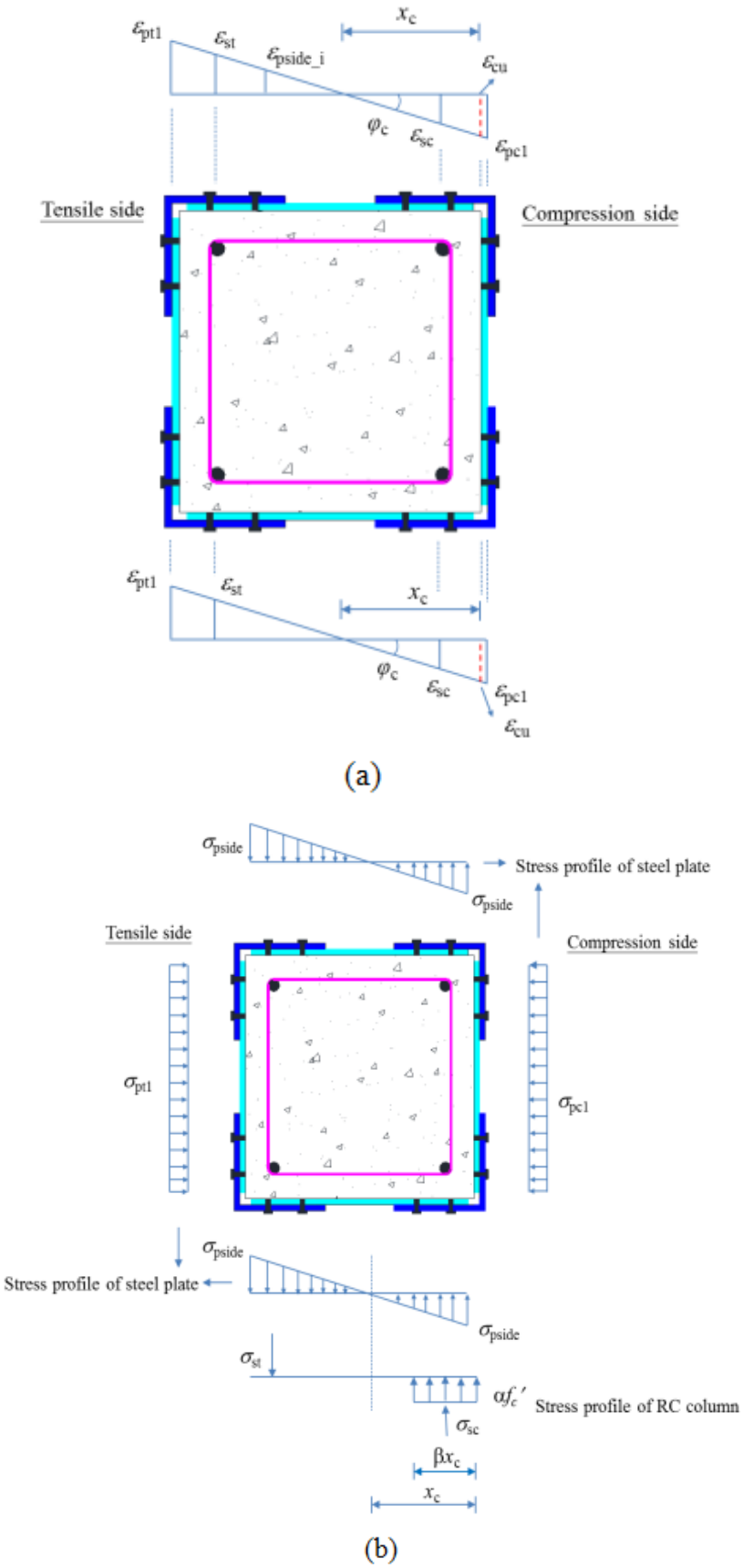

Fig. 14. (a) Strain profiles and (b) Stress profiles

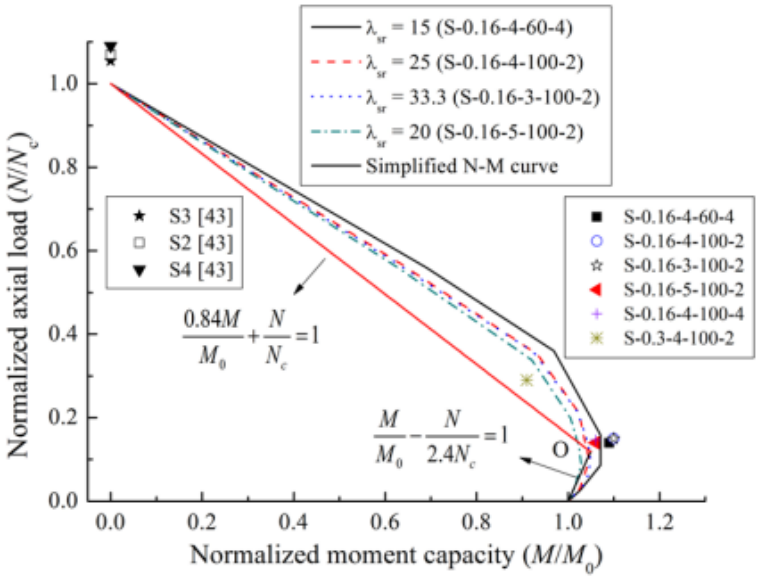

Fig. 15. N-M interaction curve

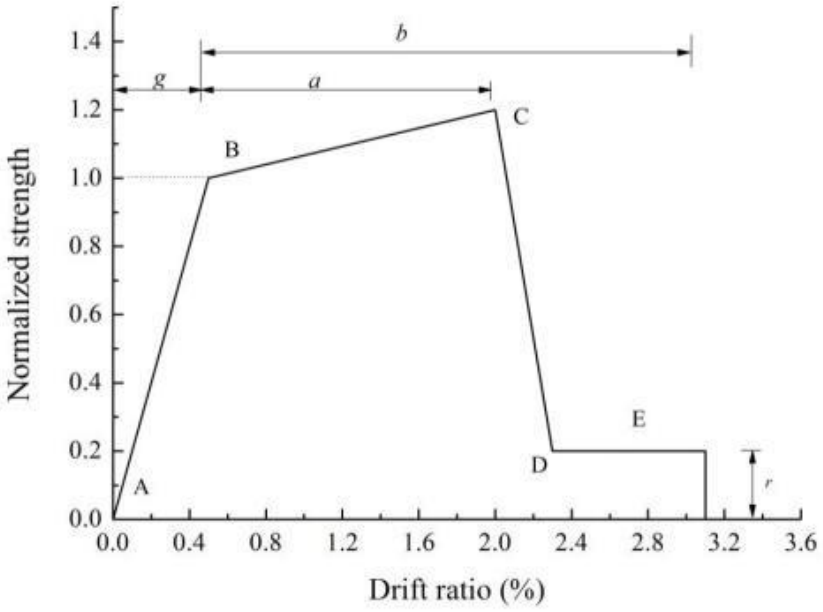

Fig. 16. Generalized force-deformation curve [44]

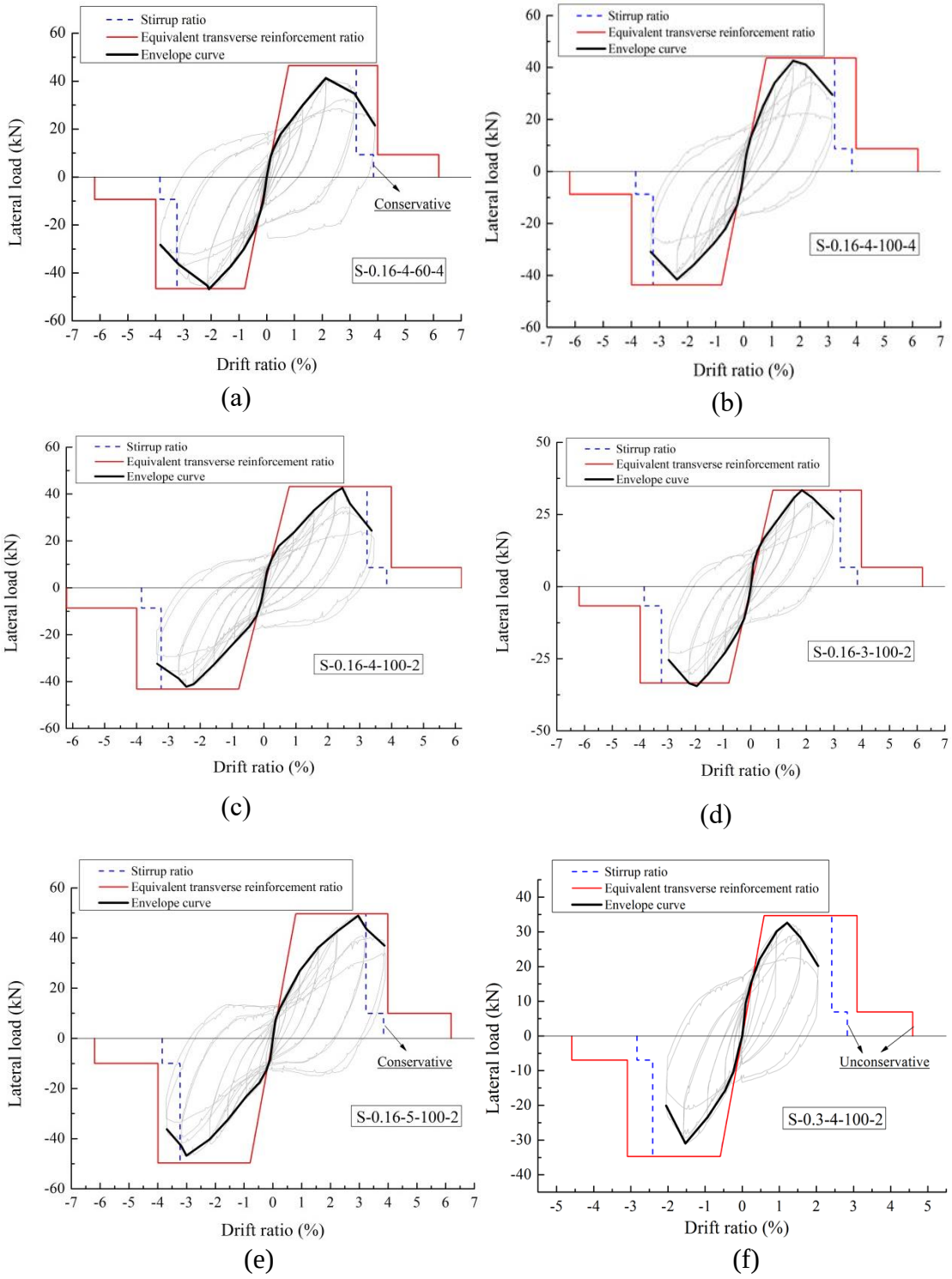

Fig. 17. Comparison of generalized force-deformation